Title

TSC1 loss increases risk for tauopathy by inducing tau acetylation and preventing tau clearance via chaperone-mediated autophagy

Journal

Science Advances, 7(45)

ISSN

2375-2548

Authors

Alquezar, Carolina
Schoch, Kathleen M
Geier, Ethan G
et al.

Publication Date

2021-11-05

DOI

10.1126/sciadv.abg3897

Peer reviewed

NEUROSCIENCE

TSC1 loss increases risk for tauopathy by inducing tau acetylation and preventing tau clearance via chaperone-mediated autophagy

Carolina Alquezar[1], Kathleen M. Schoch[2], Ethan G. Geier[3], Eliana Marisa Ramos[4], Aurora Scrivo[5], Kathy H. Li[6], Andrea R. Argouarch[1], Elisabeth E. Mlynarski[7], Beth Dombroski[7], Michael DeTure[8], Dennis W. Dickson[8], Jennifer S. Yokoyama[3], Ana M. Cuervo[5], Alma L. Burlingame[6], Gerard D. Schellenberg[7], Timothy M. Miller[2], Bruce L. Miller[1], Aimee W. Kao[1]*

Age-associated neurodegenerative disorders demonstrating tau-laden intracellular inclusions are known as tauopathies. We previously linked a loss-of-function mutation in the *TSC1* gene to tau accumulation and frontotemporal lobar degeneration. Now, we have identified genetic variants in *TSC1* that decrease TSC1/hamartin levels and predispose to tauopathies such as Alzheimer's disease and progressive supranuclear palsy. Cellular and murine models of *TSC1* haploinsufficiency, as well as human brains carrying a *TSC1* risk variant, accumulated tau protein that exhibited aberrant acetylation. This acetylation hindered tau degradation via chaperone-mediated autophagy, thereby leading to its accumulation. Aberrant tau acetylation in *TSC1* haploinsufficiency resulted from the dysregulation of both p300 acetyltransferase and SIRT1 deacetylase. Pharmacological modulation of either enzyme restored tau levels. This study substantiates *TSC1* as a novel tauopathy risk gene and includes *TSC1* haploinsufficiency as a genetic model for tauopathies. In addition, these findings promote tau acetylation as a rational target for tauopathy therapeutics and diagnostic.

INTRODUCTION

Tauopathies constitute a group of age-related neurodegenerative diseases characterized by the presence of neuronal and/or glial inclusions composed of the microtubule-binding protein tau. This group encompasses primary tauopathies, such as frontotemporal dementia (FTD), corticobasal degeneration, and progressive supranuclear palsy (PSP) where tau inclusions are the major neuropathologic abnormality, as well as secondary tauopathies, such as Alzheimer's disease (AD), where tau deposits occur in association with other pathologies (*1*). The incidence of tau-related neurodegenerative diseases is increasing, partly owing to the rise in life expectancy, but effective therapies are still lacking. Cumulative evidence from cellular and murine tauopathy models suggests that aging and aberrant posttranslational modifications (PTMs) alter the steady-state levels of tau (*2*–*5*). However, many of these studies were performed in models expressing mutant, truncated, or overexpressed forms of tau, while most human tauopathies accumulate nonmutant tau. Thus, unveiling the etiology of tauopathies requires models of endogenous nonmutant tau accumulation. The limited understanding of the molecular basis for nonmutant tau accumulation has surfaced as a key impediment to the development of diagnostics and therapies for age-associated tauopathies.

Over the past two decades, an interesting pattern has emerged in which dose-dependent mutations in the same gene can predispose to both neurodevelopmental and age-associated neurodegenerative disorders. The first gene to be recognized as such was *glucocerebrosidase A* (*GBA*), in which mutations can underlie both Gaucher's and Parkinson's disease (*6*), but many others have since been identified (*7*–*9*). Previously, we described an individual with FTD who carried a novel, monoallelic loss-of-function (LOF) mutation in the *TSC1* gene (*10*). Until this report, *TSC1* mutations had only been associated with tuberous sclerosis complex (TSC), a juvenile-onset neurodevelopmental disorder typified by seizures, cognitive delay, space-occupying tumors, and skin stigmata (*11*). As an adult-onset tauopathy gene, *TSC1* would be another gene linking disorders widely separated by age. TSC can manifest in a highly heterogeneous manner, ranging from cases characterized by early childhood onset of intractable seizures and severe developmental delay to those presenting in adulthood with only skin stigmata and mild psychiatric symptoms (*12*). We recently showed that a cohort of adults with TSC exhibited cognitive phenotypes consistent with FTD (*13*). In our earlier studies, *TSC1* mutation carriers exhibited evidence of tau accumulation in cell-based models, neuropathology, and by positivity on tau positron emission tomography (PET) imaging (*10*, *13*). Thus, clinical, genetic, experimental, and neuroimaging data all support an association of *TSC1* gene mutations with tauopathy. However, additional genetic and mechanistic evidence would solidify this association.

The major objectives of this study were to validate *TSC1* gene as a tauopathy risk factor and to unravel the mechanistic basis for tau accumulation associated with *TSC1* mutations. To do so, we leveraged the genetics of human tauopathy cohorts and identified additional *TSC1* risk variants that shorten the half-life and levels of the TSC1/hamartin protein. We also generated murine and neuronal

[1]UCSF Memory and Aging Center, Department of Neurology, University of California San Francisco, San Francisco, CA 94158, USA. [2]Department of Neurology, Washington University School of Medicine, St. Louis, MO 63110, USA. [3]Department of Radiology and Biomedical Imaging, University of California San Francisco, San Francisco, CA 94143, USA. [4]Department of Neurology, David Geffen School of Medicine, University of California Los Angeles, Los Angeles, CA 90095, USA. [5]Institute for Aging Research, Albert Einstein College of Medicine, New York, NY 10461, USA. [6]Department of Pharmaceutical Chemistry, University of California San Francisco, San Francisco, CA 94158, USA. [7]Department of Pathology and Laboratory Medicine, Penn Neurodegeneration Genomics Center, Perelman School of Medicine, University of Pennsylvania, Philadelphia, PA 19104-4238, USA. [8]Department of Neuroscience, The Mayo Clinic Florida, 4500 San Pablo Road, Jacksonville, FL 32224, USA.
*Corresponding author. Email: aimee.kao@ucsf.edu

models of *TSC1* haploinsufficiency (*TSC1*$^{+/-}$) and showed that they accumulated abnormally acetylated tau protein. This observation was validated in human tauopathy subjects carrying *TSC1* risk variants. Acetylation of tau prevented its efficient degradation in lysosomes. *TSC1* haploinsufficiency both promoted p300 histone acetyltransferase (HAT) activity and dampened SIRT1 histone deacytelase (HDAC) levels. Reversing these effects prevented tau accumulation. Collectively, this study reveals *TSC1* as a novel risk gene for tauopathies and identifies the mechanisms by which TSC1/hamartin haploinsufficiency leads to tau accumulation. These findings support preventing tau acetylation as a rational target for tauopathy therapeutics.

RESULTS

Genetic variants in the TSC1 gene are overrepresented in cohorts of sporadic tauopathy

We have previously demonstrated a link between FTD and pathogenic variants in *TSC1* (*10*, *13*). To better understand the relationship between *TSC1* and risk of tauopathies, we examined the frequency of rare *TSC1* variants in a cohort of individuals diagnosed with early-onset AD (EOAD) (*14*), which has a stronger contribution of tau pathology than its more common, late-onset counterpart. The EOAD cohort showed an enrichment of the rare variant in *TSC1* rs2234980 dupTGC (also known as rs118203743), relative to controls from the Genome Aggregation Database (gnomAD v2.1.1) (minor allele frequency, MAF EOAD = 0.0066 versus MAF gnomAD = 0.00006). This variant results in a serine duplication at position 1043 (S1043dup) of the TSC1/hamartin protein. In light of this finding, we screened for *TSC1* variants in a cohort of pathologically confirmed PSP cases, compared with a control cohort from the Alzheimer's Disease Sequencing Project (ADSP) Discovery dataset. The *TSC1* S1043 duplication (rs2234980) variant was also enriched in PSP cases, although not significantly (*P* value = 0.4618, odds ratio = 1.897). In addition, another rare-coding variant in the *TSC1* gene (rs118203742), resulting in a glycine-to-serine change at position 1035 of the protein (G1035S), was found to be significantly associated with PSP (*P* value = 0.031, odds ratio = 4.241; Fig. 1A). Sanger sequencing analysis confirmed the presence of the variants and showed that both were heterozygous. These results demonstrated that the *TSC1* gene could be associated with increased risk for tauopathies.

The *TSC1* gene encodes a 1164–amino acid protein known as TSC1/hamartin. Both the rs2234980 and rs118203742 variants introduce serine residues in a region of TSC1/hamartin that we identified as a potential PEST motif (ePESTfind tool) (Fig. 1B) (*15*). PEST motifs are amino acid sequences enriched with proline (P), glutamate (E), serine (S), and threonine (T) residues that regulate protein degradation via the proteasome (*15*). Given their localization, we posited that the tauopathy-associated *TSC1* variants could exert a LOF effect by accelerating TSC1/hamartin degradation in the proteasome. To test this possibility, we generated cell lines expressing tagged versions of wild-type (WT) or variant TSC1/hamartin. Cells were treated with cycloheximide (CHX) to halt protein synthesis and the half-life of WT and variant TSC1/hamartin proteins was measured over time. Both of the tauopathy-associated *TSC1* genetic variants shortened TSC1/hamartin protein half-life by nearly 30% (Fig. 1C). To confirm that the genetic variants accelerate the proteasomal degradation of TSC1/hamartin, we blocked the proteasome, using MG132, after inhibiting protein synthesis with CHX. Proteasome inhibition decreased the turnover of TSC1 protein (Fig. 1, D and E), suggesting that TSC1/hamartin is indeed degraded in the proteasome and that genetic variants within the PEST motif accelerate the proteasomal degradation of TSC1/hamartin. In addition, we compared TSC1 protein levels from neuropathological tissue of PSP subjects carrying the G1035S variant in *TSC1* to healthy controls (table S1). Consistent with the cell-based experiments, TSC1/hamartin levels were decreased in the individuals carrying the G1035S variant (Fig. 1F). These results suggested that genetic variants decreasing TSC1/hamartin levels are associated with tauopathies.

iNeuron models of TSC1 haploinsufficiency accumulate tau

We have previously shown that *TSC1* haploinsufficiency results in specific tau accumulation in the SH-SY5Y neuronal-like cell line (*10*). However, it remained unknown whether *TSC1* haploinsufficiency also induced tau accumulation in induced pluripotent stem cell (iPSC)–differentiated iNeurons. To assess this, we generated *TSC1* haploinsufficient iPSCs. We obtained fibroblasts from three members of a family carrying a heterozygous LOF mutation in *TSC1* (p.Arg22CysfsTer5) associated with FTD and tau accumulation, as well as one WT control family member (*10*) (fig. S1). The fibroblasts were reprogrammed into iPSCs, differentiated into iNeurons, and compared to a well-characterized WT iPSC line (F11350) (table S2). As expected, TSC1/hamartin levels were decreased in the iNeurons carrying the p.Arg22CysfsTer5 *TSC1* mutation, compared to WT controls. In addition, *TSC1* mutant iNeurons exhibited increased tau levels compared to controls (Fig. 1G).

Although the patient-derived cell lines are a useful proof of concept that humanized neuronal models of *TSC1* haploinsufficiency also accumulate tau, these lines suffer from the limitation of differences in genetic background. Thus, we used CRISPR-Cas9 genome editing to generate *TSC1* haploinsufficient (*TSC1*$^{+/-}$) lines in the background of the PGP1 WT parent iPSC line (fig. S2 and table S2). The resulting iPSC lines were isogenic at all but the *TSC1* locus. Two independent *TSC1*$^{+/-}$ clones were generated, differentiated into iNeurons, and used to assess tau compared to the parent line. Similar to the *TSC1* family cell lines, these *TSC1*$^{+/-}$ neurons demonstrated increased tau levels compared to an isogenic control (Fig. 1H). Thus, *TSC1* haploinsufficiency induced tau accumulation in both patient-derived and genome-edited iPSC-derived neuronal lines, supporting the results previously found in *TSC1*$^{+/-}$ SH-SY5Y cells.

Tau accumulation in TSC1 haploinsufficiency is not a consequence of impaired macroautophagy activity

One of the functions of TSC1/hamartin protein is to stabilize TSC2/tuberin (*16*), a guanosine triphosphatase–activating protein that negatively regulates mTOR (mammalian target of rapamycin) pathway (*16*). *TSC1* haploinsufficiency leads to TSC2/tuberin degradation and mTOR complex 1 (mTORC1) overactivation (fig. S3A). The mTORC1 pathway controls important cellular functions including protein degradation through autophagy (*17*), and thus, overactivation of mTORC1 down-regulates autophagy and impairs protein degradation (fig. S3A). It has been demonstrated that tau protein is degraded in lysosomes via autophagy (*18*, *19*). In this context, we wondered whether tau accumulation in *TSC1* haploinsufficiency was due to an overall decrease in protein degradation through the autophagy pathway (autophagic flux) because of abnormal mTORC1 activation.

To evaluate this possibility, we considered macroautophagy, the best characterized type of autophagy, and measured autophagic flux in a series of fibroblasts with and without a LOF mutation in *TSC1*

A

Diagnosis	Variant in TSC1 gene	Amino acid change	Ref allele	Alt allele	Case AF	Control AF	Odds ratio	*P* value
PSP	rs2234980	S1043dup	$(GCT)_6GC$	dupTGC	0.000998	0.000526	1.896603	0.461808
PSP	rs118203742	G1035S	C	T	0.004444	0.001052	4.24171	0.030767

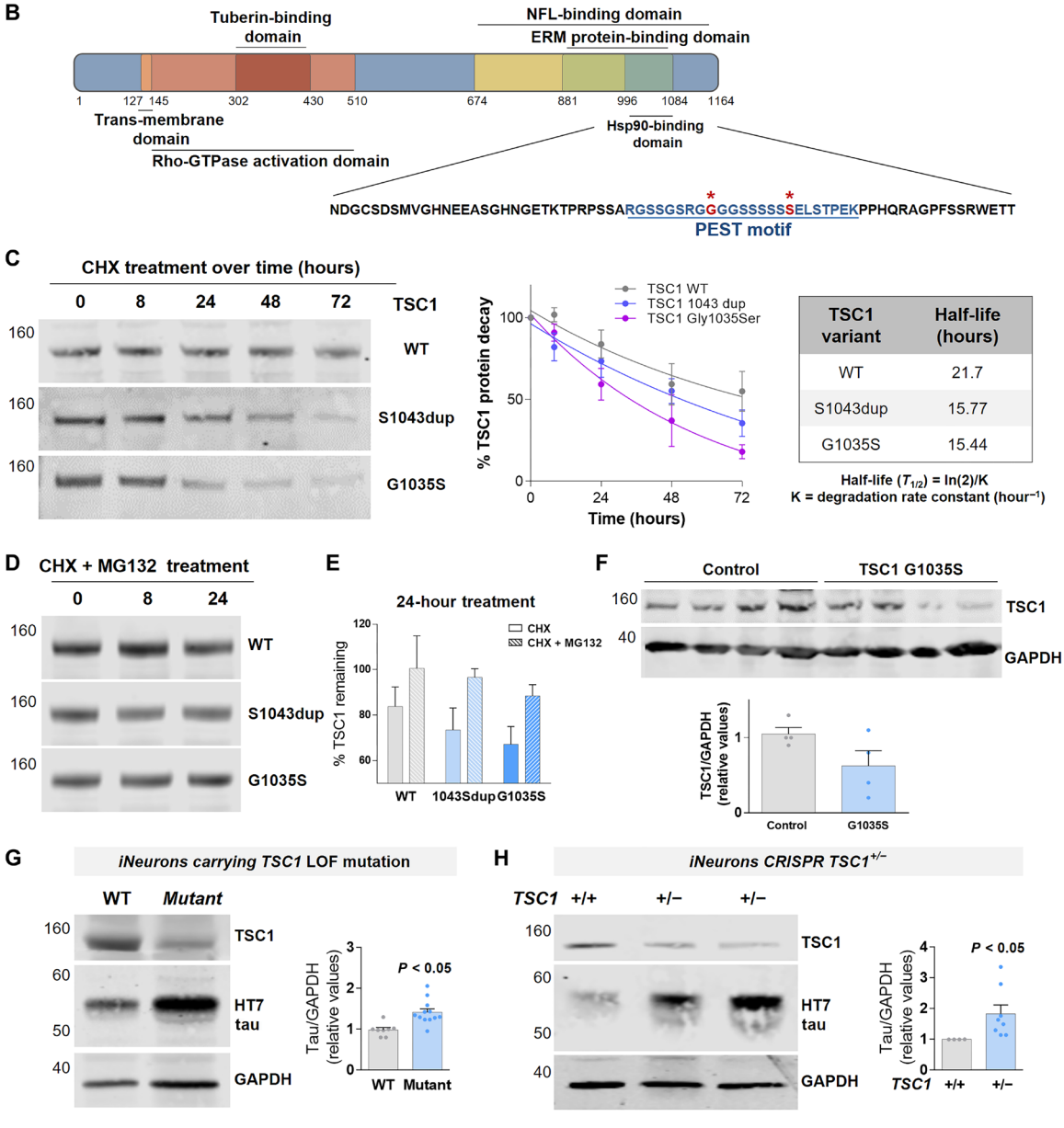

Fig. 1. Genetic variants in *TSC1* are overrepresented in tauopathy patients. (**A**) *TSC1* genetic variants found in PSP subjects, compared to healthy control individuals from the ADSP database. (**B**) Representation of TSC1/hamartin protein with the PEST motif indicated in blue and the disease-associated variants in red. (**C**) Immunoblots showing TSC1-FLAG levels after the CHX time-course treatment. The plot and the table represent TSC1/hamartin half-life. (**D**) Immunoblots showing TSC1-FLAG levels at 8 and 24 hours after CHX and MG132 treatments. (**E**) Quantification of the effect of proteasome in the clearance of WT and mutant TSC1. (**F**) Immunoblot showing decreased TSC1/hamartin levels in the brain of PSP subjects carrying the G1035S variant in *TSC1* gene. (**G** and **H**) TSC1/hamartin and tau levels in iNeurons derived from a family carrying a *TSC1* LOF mutation (p.Arg22CysfsTer5) (G) and isogenic *TSC1*$^{+/-}$ induced pluripotent stem cells (iPSCs) generated in the background of the PGP1 line (H). (G) Immunoblots show two representative individuals (MHF130 WT and MHF104 mutant). The quantification is the mean ± SEM of four independent experiments including two WT (MHF130 and F11350) and three mutant lines (MH104, MH128, and MHF129). (H) Plot shows the mean ± SEM of four independent experiments. Statistical significance was assessed by Student's *t* test. GAPDH, glyceraldehyde-3-phosphate dehydrogenase.

(fig. S3, B and C) (*10*). Cells were transduced with lentivirus carrying an mCherry–green fluorescent protein (GFP)–LC3 tandem construct that allows measuring autophagic flux as the maturation of autophagosomes (vesicles positive for mCherry and GFP fluorescence) into autolysosomes (vesicles in which GFP fluorescence is lost because of acidification upon fusion with lysosomes) (*20*). Fibroblasts carrying the *TSC1* mutation ($TSC1^{+/-}$) demonstrated higher abundance of autophagic vacuoles (overall autophagic compartments independently of their maturation state). This increase was driven, for the most part, by autolysosomes, supporting an increase, rather than a decrease, in macroautophagic flux associated with *TSC1* haploinsufficiency (Fig. 2A and fig. S3D).

Overactivation of autophagy has been previously reported in early stages of AD (*21*), where it has been proposed to have a compensatory, neuroprotective role. To address whether *TSC1* haploinsufficiency caused a compensatory macroautophagy activation in neuronal cells, we measured the levels of LC3-II protein in differentiated SH-SY5Y cells before and after treatment with bafilomycin (Baf1), a V–adenosine triphosphatase (ATPase) inhibitor that blocks protein degradation in the lysosomes. This approach provides an estimate of protein degradation through the autophagy-lysosome system (*22*). $TSC1^{+/-}$ SH-SY5Y cells exhibited increased LC3-II in the basal state, which further increased after Baf1 treatment (Fig. 2B). These results confirmed that in both fibroblasts and differentiated SH-SY5Y cells, *TSC1* haploinsufficiency caused a compensatory enhancement in autophagic flux, rather than inhibition, as would be expected as a result of the aberrant mTORC1 activation previously demonstrated (*10*).

Several studies have reported that mTOR activation is associated with neurodegenerative diseases (*23*), and thus, we next asked whether mTOR was required for tau accumulation in $TSC1^{+/-}$ cells. mTOR is the catalytic subunit of two distinct protein complexes, mTORC1 and mTORC2. Control and $TSC1^{+/-}$ cells were treated with the mTORC1 inhibitor rapamycin and the dual mTORC1/2 inhibitor torin-1. While mTORC1 inhibition with rapamycin did not prevent tau accumulation in $TSC1^{+/-}$ cells, the inhibition of both mTORC1 and mTORC2 with torin-1 significantly decreased tau levels in TSC1 insufficient cells (Fig. 2C). mTORC1 and mTORC2 inhibition was assessed by the phosphorylation status of P70S6K and AKT proteins, respectively (fig. S3E). These results suggested that the complete inhibition of both mTORC1 and mTORC2 complexes was required to reduce tau accumulation in *TSC1* haploinsufficient cells.

TSC1/hamartin haploinsufficiency prevents tau degradation by chaperone-mediated autophagy

Since tau accumulation in $TSC1^{+/-}$ cells was not due to a general decrease in autophagy, we next investigated how TSC1/hamartin specifically regulates tau levels. Protein levels can be regulated via production or degradation; therefore, we first determined whether tau expression changes in $TSC1^{+/-}$ cells. Tau (*MAPT*) mRNA levels were assessed by quantitative polymerase chain reaction (qPCR) in differentiated SH-SY5Y cells. $TSC1^{+/-}$ cells showed no difference in tau mRNA expression compared to controls (Fig. 3A).

We then turned our attention to tau clearance. Chaperone-mediated autophagy (CMA) is a form of selective protein degradation that requires recognition of a KFERQ motif by the Hsc70 chaperone and subsequent binding and translocation of the targeted protein into the lysosomes through the Lamp2A (lysosome-associated membrane

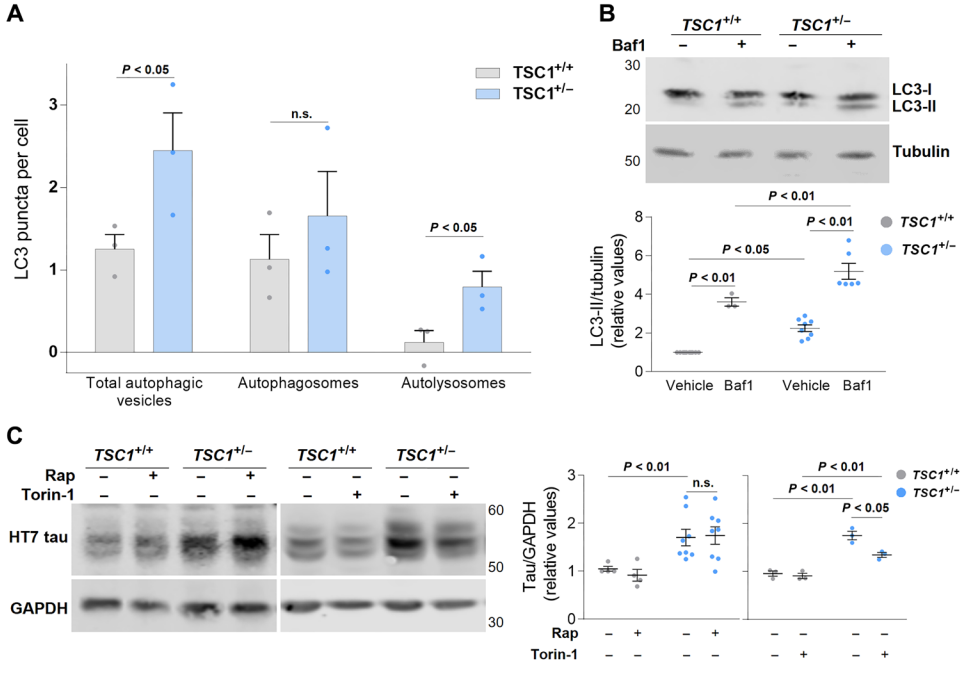

Fig. 2. TSC1/hamartin haploinsufficiency induces tau accumulation independent of macroautophagy impairment and mTORC1 pathway activation. (**A**) Plot showing the number of LC3-II puncta per cell in $TSC1^{+/+}$ and $TSC1^{+/-}$ fibroblasts. Total autophagic vesicles consist of autophagosomes and autolysosomes. n.s., not significant. (**B**) Anti-LC3 immunoblot showing LC3-I and -II levels before and after 6 hours of treatment with 100 nM bafilomycin 1 (Baf1) in control or $TSC1^{+/-}$-differentiated SH-SY5Y cells. (**C**) Immunoblots showing tau levels before and after 72 hours of treatment with rapamycin (Rap, 25 nM) or Torin-1 (50 nM) in WT and $TSC1^{+/-}$-differentiated SH-SY5Y cells. All plots show the means ± SEM from at least three independent experiments. Two-way analysis of variance (ANOVA) tests followed by Bonferroni's comparison was used to assess statistical significance. Unless otherwise indicated, *P* values indicate comparison to the first, leftmost column in the graph.

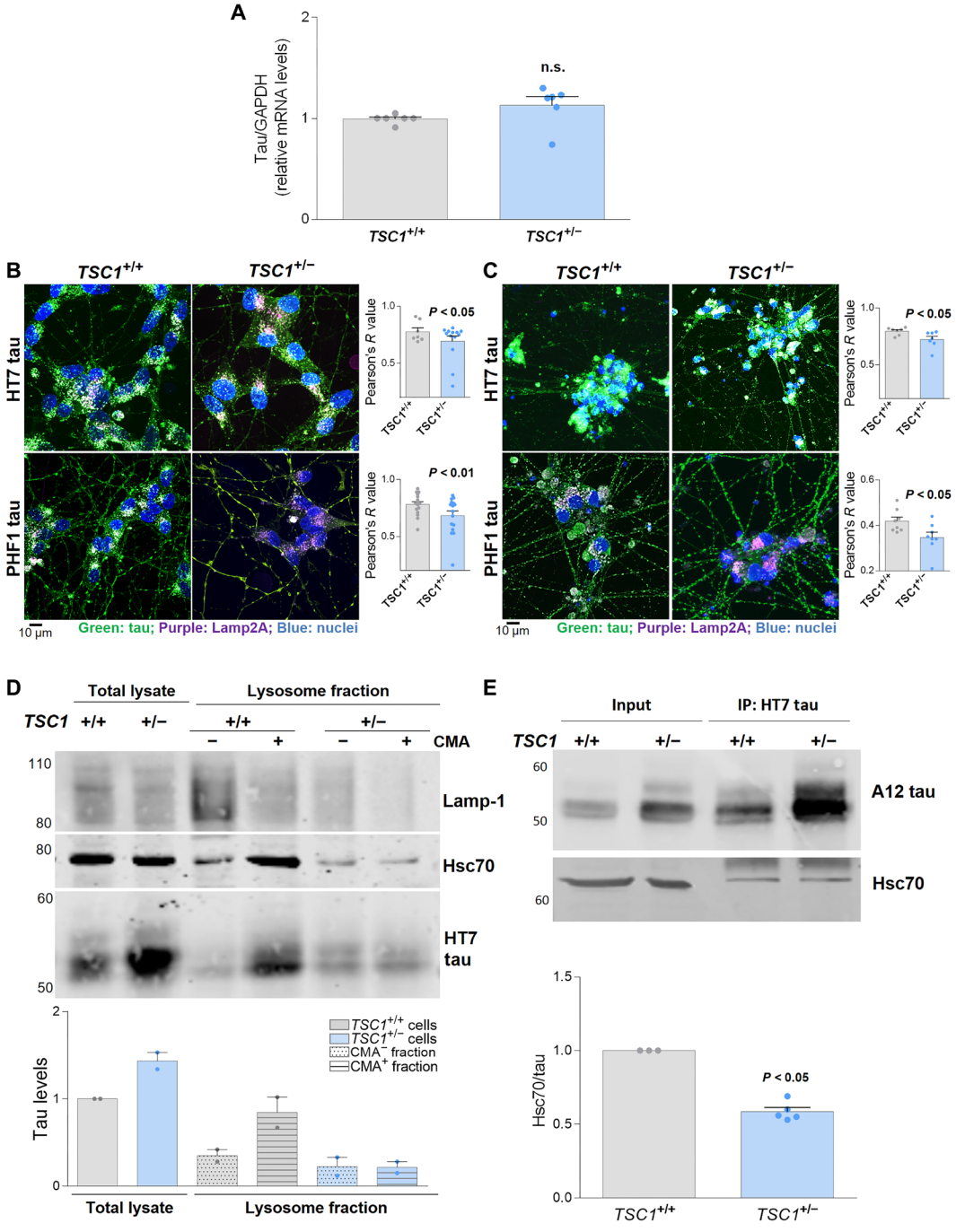

Fig. 3. Loss of TSC1/hamartin impairs tau degradation in the lysosomes by CMA. (**A**) Tau mRNA levels in WT and *TSC1*$^{+/-}$-differentiated SH-SY5Y cells measured by qPCR. (**B** and **C**) Control and *TSC1*$^{+/-}$-differentiated SH-SY5Y cells (B) and iNeurons (C) immunostained with antibodies against tau (green) and the lysosomal marker Lamp2A (purple). Nuclei were stained with 4′,6-diamidino-2-phenylindole (DAPI) (blue). The imaging experiments were performed in triplicates. Plots show the average of Pearson's *R* correlation value for both channels and the two tau antibodies. The statistical significance was assessed by Student's *t* test. (**D**) CMA active (+) and CMA inactive (−) lysosomal fractions were isolated from control and *TSC1*$^{+/-}$-differentiated SH-SY5Y cells. Representative immunoblots showing the distribution of tau protein in the lysosomal compartments are shown. Lamp-1 and Hsc70 were used as markers for CMA^{-} lysosomes and CMA^{+} lysosomes, respectively. Plot shows the means ± SEM of tau levels from two independent experiments. (**E**) Tau protein was immunoprecipitated from *TSC1*$^{+/+}$ and *TSC1*$^{+/-}$ cells using a monoclonal anti-tau antibody (HT7). The plot shows the quantification of Hsc70/tau coimmunoprecipitation. The experiment was performed three times. Student's *t* test was used to assess statistical significance.

protein type 2A) channel (*24*). Tau contains two KFERQ motifs and thus is a client for CMA (*19*). To understand whether *TSC1* haploinsufficiency impairs tau degradation in lysosomes, control and $TSC1^{+/-}$ SH-SY5Y cells (Fig. 3B and fig. S4) and iNeurons (Fig. 3C and fig. S5) were immunostained with tau and Lamp2A antibodies. $TSC1^{+/-}$ cells showed decreased tau/Lamp2A colocalization compared with $TSC1^{+/+}$ cells (Fig. 3, B and C, and figs. S4 and S5), suggesting that *TSC1* haploinsufficiency resulted in impaired tau association with CMA-competent lysosomes. To directly test this, we performed biochemical separation of lysosome fractions (*25*). CMA-enriched (CMA^+) and CMA-nonenriched (CMA^-) lysosomes were isolated from control and $TSC1^{+/-}$ cells and then were immunoblotted for tau. The lysosomal membrane protein Lamp1 and the CMA-specific chaperone Hsc70 were used as markers of CMA^- and CMA^+ fractions, respectively. *TSC1* haploinsufficiency led to a pronounced decrease of tau levels in CMA^+ lysosomes (Fig. 3D). In addition, in $TSC1^{+/-}$ cells, relatively less Hsc70 coimmunopreciptated with tau (Fig. 3E). Together, these results suggest that tau degradation via CMA is compromised in $TSC1^{+/-}$ cells. TSC1/hamartin insufficiency did not alter the levels of glyceraldehyde-3-phosphate dehydrogenase (GAPDH) (fig. S6), a well-known CMA subtract (*26*), implying that the loss of TSC1/hamartin protein specifically impaired tau degradation.

Tau from $TSC1^{+/-}$ cells undergoes aberrant acetylation that affects its degradation

Tau undergoes many PTMs that affect its function and steady-state levels (*5*). PTMs have the potential to directly regulate tau degradation via the proteasome and lysosomes (*5*). To explore whether *TSC1* haploinsufficiency affected tau PTMs, we performed tau immunoprecipitation followed by mass spectrometry analysis. The residues phosphorylated on tau were not different in $TSC1^{+/-}$ cells compared to controls (fig. S7A). Furthermore, although the accumulated tau in $TSC1^{+/-}$ cells was phosphorylated, the phospho-tau/total-tau ratio was equal in $TSC1^{+/+}$ and $TSC1^{+/-}$ cells (fig. S7B), suggesting that TSC1/hamartin loss did not increase tau phosphorylation. On the other hand, compared to WT cells, tau extracted from $TSC1^{+/-}$ cells was uniquely acetylated on six lysine (K) residues: K150, K240, K343, K369, K375, and K385 (Fig. 4, A and B, and fig. S8). K174 was acetylated in both control and $TSC1^{+/-}$ cells. Notably, *TSC1* insufficiency did not alter acetylation of TDP-43 (fig. S9), an FTD-linked protein that has been shown to be acetylated in some neurodegenerative disease (*27*).

Abnormal acetylation of tau has been reported to interfere with tau levels and function by impairing its degradation and disrupting its ability to stabilize microtubules (*3*, *4*). A recent report demonstrated that tau multi-acetylation remarkably reduces its degradation via CMA in vitro (*28*). Therefore, we asked whether TSC1-related tau acetylation also prevented tau degradation by CMA. To do so, we generated cell lines stably expressing WT tau or tau in which the six acetylated lysine residues in $TSC1^{+/-}$ cells were mutated to either acetyl-mimetic glutamine residues (6K➔Q Tau) or non-acetylatable arginine residues (6K➔R Tau). If lysine acetylation prevented CMA-mediated degradation, one would predict that tau colocalization with the CMA marker Lamp2A would decrease. Tau and Lamp2A colocalization decreased in cells expressing 6K➔Q acetyl-mimetic tau but not in cells expressing non-acetylatable 6K➔R tau (Fig. 4C and fig. S10). To verify that TSC1-mediated tau acetylation disrupted its degradation via CMA, we assessed the binding of acetyl-mimetic tau and non-acetylatable tau to Hsc70. As expected, TSC1-mediated tau acetylation reduced tau/Hsc70 binding (Fig. 4D).

Tau acetylation has been shown to disrupt its ability to stabilize microtubules and also alter its phosphorylation status, leading to tau accumulation and aggregation (*4*, *29*, *30*). The specific acetyl-mimetic residues found in 6K➔Q tau did not disrupt tau binding to microtubules or alter its phosphorylation (fig. S11). While acetylation on different lysine residues likely has distinct effects, our data suggested that the mechanistic basis for tau accumulation in *TSC1* haploinsufficiency was a specific acetylation pattern that subsequently disrupted tau degradation by CMA.

TSC1/hamartin induces tau acetylation via p300 HAT and SIRT1 HDAC

Acetyl groups are conferred onto tau protein by HATs such as p300 and are removed by deacetylases (HDACs) such as SIRT1, HDAC3, and HDAC6 (*3*, *4*, *31*–*33*). To better understand the process of tau acetylation in *TSC1* haploinsufficiency, we measured p300 HAT activity and HDAC levels in RA-differentiated SH-SY5Y. $TSC1^{+/-}$ cells showed increased p300 HAT activity, as measured indirectly by the acetylation of histone 3 on lysine 18 ($H3^{acK18}$) (Fig. 5A) and directly with a specific enzymatic assay (Fig. 5B). Accompanying the increased p300 acetylase activity, $TSC1^{+/-}$ cells exhibited reduced protein and mRNA levels of the SIRT1 HDAC (Fig. 5, C and D), but the levels of HDAC3 and HDAC6 were not affected (fig. S12). Similar to SH-SY5Y cells, $TSC1^{+/-}$ iPSC-iNeurons also showed increased tau acetylation and dysregulation of p300 and SIRT1 (Fig. 5, E to G). Overall, TSC1 haploinsufficiency both enhanced p300 acetyltransferase and decreased SIRT1 deacetylase activity, resulting in a net increase in tau acetylation.

We next asked whether modulation of p300 HAT and SIRT1 HDAC affected tau accumulation in *TSC1* haploinsufficiency by pharmacologically inhibiting p300 HAT activity (with A485) (*34*) or activating SIRT1 deacetylase (with resveratrol, RSV) (*35*). Both treatments effectively reduced tau acetylation in $TSC1^{+/-}$ cells (Fig. 6A). Blocking tau acetylation decreased total tau levels in $TSC1^{+/-}$ cells without affecting tau phosphorylation at S396/S404 (Fig. 6A). Tau mRNA levels were unaffected (fig. S13A). Treatment with the p300 HAT inhibitor increased SIRT1 mRNA and protein levels (Fig. 6B and fig. S13B), suggesting that p300 regulated SIRT1 expression. Therefore, A485 treatment may decrease tau both directly, via blocking p300 activity, and indirectly, by increasing SIRT1 levels. The inhibition of mTORC1 and mTORC2 with torin-1 mimicked the effect of A485 and RSV in decreasing tau acetylation and levels (Fig. 6C). This result suggested that TSC1/hamartin could regulate p300 HAT activity by its role as an mTOR modulator.

To verify that tau accumulation in *TSC1* insufficiency was driven by acetylation and not phosphorylation, we treated cells with AZD1080, a GSK3-kinase inhibitor known to block tau phosphorylation. In contrast to the inhibition of tau acetylation, AZD1080 treatment did not normalize tau levels in $TSC1^{+/-}$ cells (Fig. 6D), suggesting that acetylation but not phosphorylation triggered tau accumulation in *TSC1* insufficiency. Together, these data demonstrated that tau accumulation in *TSC1* haploinsufficient cells resulted from increased tau acetylation and that preventing tau acetylation normalized tau levels.

TSC1/hamartin haploinsufficiency induces tau acetylation and neurodegeneration in vivo

To determine whether TSC1/hamartin affected tau levels and PTMs in vivo and in an age-dependent manner, we generated a model of

A

Lysine	Peptide	e-value
K150	TKIATPR	0.0019
K240	TPPKSPSSAKSR	0.0022
K343	SEKLDFKDR	2.3×10^{-4}
K369	IGSLDNITHVPGGGNKK	6.3×10^{-10}
K375	KIETHKLTFR	7.3×10^{-4}
K385	AKTDHGAEIVYK	2.0×10^{-6}

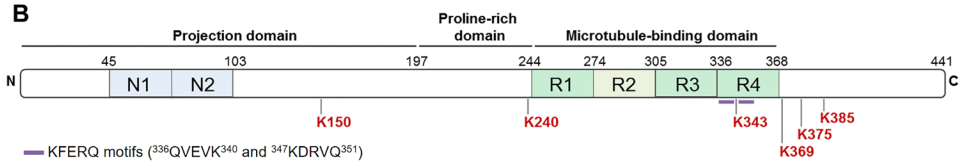

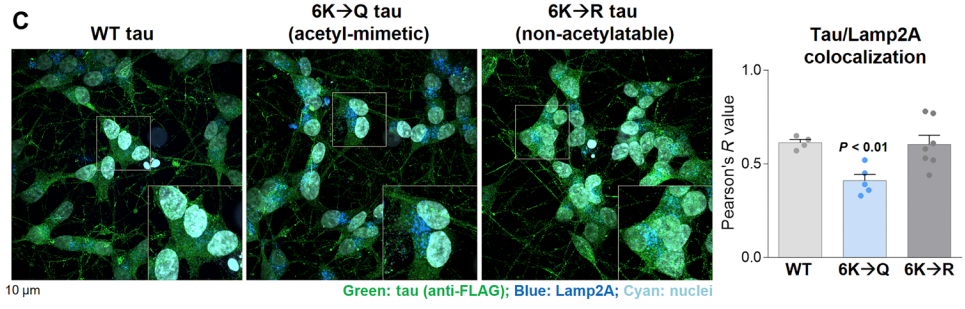

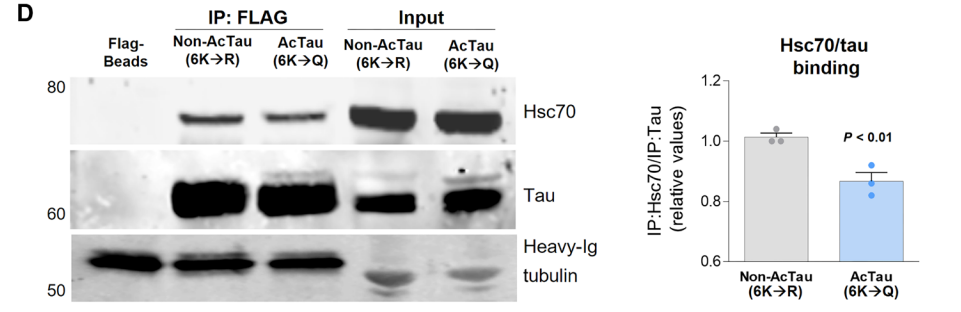

Fig. 4. TSC1-mediated tau acetylation alters the association of tau with CMA lysosomes. (**A**) List of the acetylated lysine (K) residues found by mass spectrometry in *TSC1*$^{+/-}$ but not WT SH-SY5Y cells. The expectation value (e-value), a measure of the statistical significance of a peptide assignment, is also shown. (**B**) Diagram of tau protein annotated with the functional domains, KFERQ motifs, and the acetyl-lysine residues. (**C**) SH-SY5Y cells expressing FLAG-tagged WT 2N4R tau, acetyl-mimetic tau (2N4R 6K➔Q tau), and non-acetylatable tau (2N4R 6K➔R tau) were stained with anti-FLAG and anti-Lamp2A antibodies that recognized overexpressed tau (green) and endogenous Lamp2A (dark blue), respectively. Nuclei were stained with DAPI (cyan). Plot shows the average of Pearson's *R* correlation value. Statistical significance was assessed using one-way ANOVA. (**D**) Acetyl-mimetic and non-acetylatable tau was immunoprecipitated using anti-FLAG magnetic beads. The immunoblots show the levels of Hsc70 and tau proteins in the whole lysate (input) and after the immunoprecipitation. Immunoglobulin (Ig) heavy chain and tubulin were used as loading controls for the immunoprecipitation and input, respectively. The plot shows the quantification of Hsc70/tau coimmunoprecipitation. The experiment was performed three times. Student's *t* test was used to assess statistical significance.

neuronal *TSC1* haploinsufficiency in the background of mice expressing human tau (hTau) in the absence of mouse tau (*hTau;Tsc1*^{Syn1}CKO). First, we assessed whether *TSC1* haploinsufficiency induced tau accumulation using the PHF1 tau antibody as a reflection of total tau pathology. At 6 months of age, *Tsc1*^{Syn1}CKO animals were not significantly different from controls relative to tau staining. However, at 15 months, *Tsc1*^{Syn1}CKO mice demonstrated a significant accumulation of tau protein in the somatosensory cortex and the retrosplenial cortex (RSCx; Fig. 7A and fig. S14A). The latter region is involved in hippocampal-cortex circuitry that functions in spatial cognition and memory (*36*, *37*) and that is affected early in tauopathies such as AD (*38*). To further confirm TSC1-driven pathology, soluble and insoluble tau species were fractionated from 15-month-old mice RSCx lysates. Despite clear changes in steady-state levels of tau, tau solubility was not significantly altered in the RSCx of *Tsc1*^{Syn1}CKO mice compared to controls at this age (fig. S14B).

Next, we assessed whether the tau accumulation observed in 15-month-old animals correlated with behavioral abnormalities. The auditory conditioning test measures associative memory, represented by the decrease of the freezing time in response to auditory

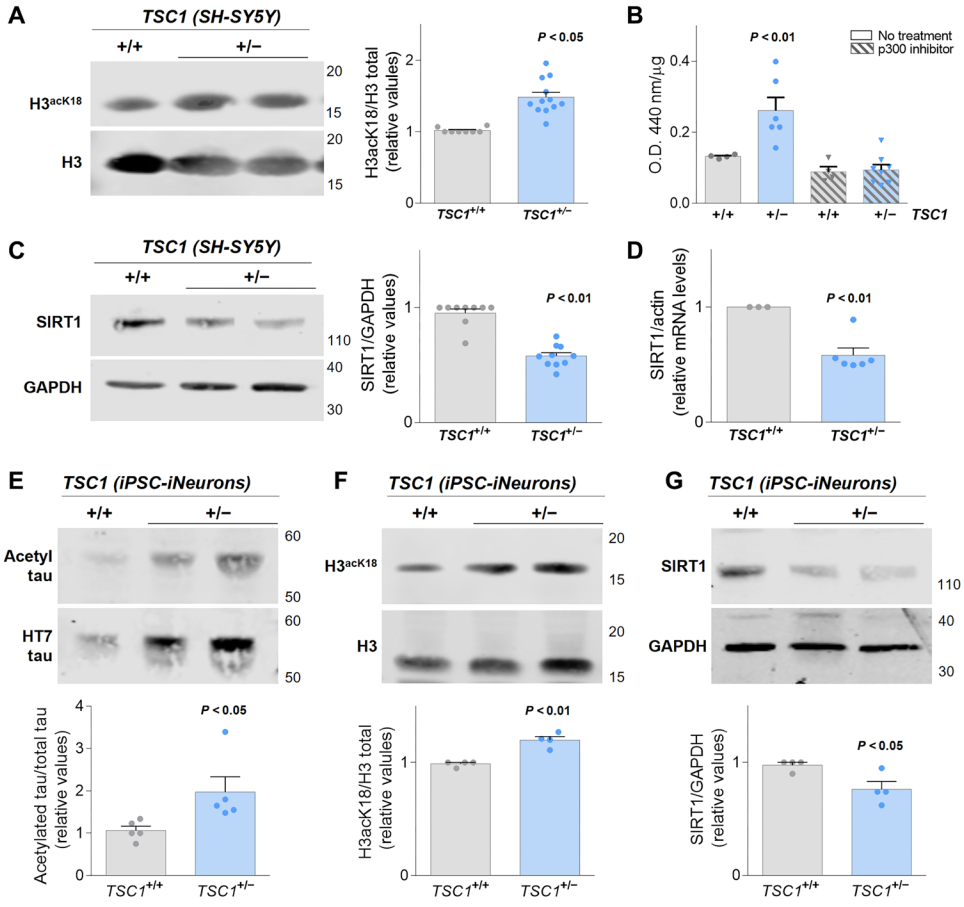

Fig. 5. TSC1/hamartin insufficiency regulates p300 HAT activity and SIRT1 HDAC levels in SH-SY5Y cells and iNeurons. (**A**) p300 HAT activity in control and *TSC1*$^{+/-}$-differentiated SH-SY5Y cells indirectly assessed by the levels of histone 3 (H3) acetylated at lysine 18 (H3^{acK18}). (**B**) Enzymatic activity of HAT in differentiated SH-SY5Y cells before and after the treatment with a specific p300 inhibitor. (**C** and **D**) SIRT1 protein (C) and mRNA levels (D) measured in control and *TSC1*$^{+/-}$-differentiated SH-SY5Y cells. (**E**) Immunoblot showing tau acetylation in *TSC1*$^{+/+}$ and *TSC1*$^{+/-}$ iPSC-derived iNeurons. (**F** and **G**) Immunoblots showing the p300 activity, assessed by the levels of H3^{acK18}, and SIRT1 levels in *TSC1*$^{+/+}$ and *TSC1*$^{+/-}$ iPSC-derived iNeurons. All experiments were performed at least in triplicate. Plots show the means ± SEM for each experiment. Statistical significance was assessed using Student's *t* test or two-way ANOVA followed by Bonferroni's comparison.

conditioning (*39*). Compared to controls, *Tsc1*^{Syn1}CKO mice showed a significant reduction in freezing time after auditory conditioning (Fig. 7B), suggesting that *TSC1* insufficiency led to associative memory impairment. Furthermore, the nesting test was used to estimate executive function of the animals. Nesting ability was measured on the basis of qualitative scoring of amount of torn nestlet material and nest shape (0 to 7 numerical scale) (*40*). *Tsc1*^{Syn1}CKO mice showed decreased nesting scores compared with control mice (Fig. 7C), supporting impaired executive function in these animals akin to what is seen in human FTD.

We also evaluated whether loss of TSC1/hamartin protein induced tau acetylation in vivo, similar to that observed in *TSC1*$^{+/-}$ neuronal cells. We used the in-house generated tau acetyl-lysine 343 antibody (AcK343) (fig. S15) to measure the levels of acetylated tau in mice RSCx lysates by immunoblot (Fig. 7D) and in tissue by immunostaining (Fig. 7E). Tau^{acK343} levels were notably increased in 15-month-old *Tsc1*^{Syn1}CKO animals compared to controls (Fig. 7, D and E). Consistent with results from *TSC1*$^{+/-}$ cells, *Tsc1*^{Syn1}CKO mice also demonstrated increased p300 HAT activity and decreased levels of SIRT1 HDAC (Fig. 7F). These results confirmed that *TSC1* haploinsufficiency led to acetyl-tau accumulation and behavioral impairments in vivo in an age-dependent manner.

Tau acetylation correlates with TSC1 insufficiency in human brains

Using Tau-PET imaging, we previously demonstrated that *TSC1* LOF mutations induce tau accumulation in the brain of affected individuals (*13*). Here, we investigated whether *TSC1* insufficiency also induces tau acetylation in humans. Postmortem brain tissue from four healthy control individuals and four pathology-confirmed PSP subjects carrying the G1035S variant in *TSC1* was evaluated for tau acetylation using the AcK343 antibody. Immunoblotting showed that TSC1/hamartin loss correlated with increased acetylation of tau at K343 (Fig. 8). Tau hyperacetylation also correlated with increased p300 HAT activity and decreased SIRT1 levels. The samples with lower TSC1/hamartin levels (P3 and P4, red dots) exhibited higher tau acetylation and p300 activity and lower SIRT1 levels. While these results were not statistically significant, these consistent trends of lower TSC1/hamartin levels being associated with the presence of acetylated tau and the dysregulation of p300/SIRT1 were intriguing

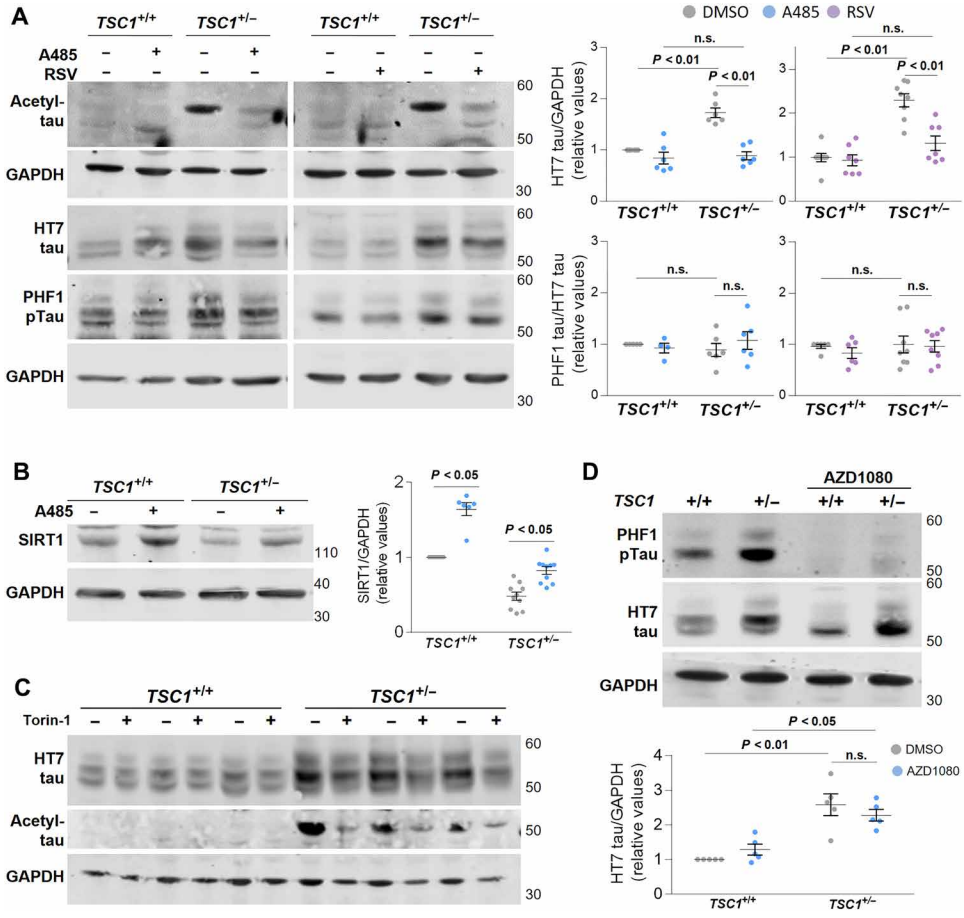

Fig. 6. Blocking tau acetylation restores tau levels in *TSC1*$^{+/-}$ cells. (**A**) Control and *TSC1*$^{+/-}$ differentiated SH-SY5Y cells were treated for 72 hours with a specific p300 inhibitor, A485 (15 μM), or with the SIRT1 activator, resveratrol (RSV) (25 μM). Immunoblots show the effect of these treatments on tau acetylation, phosphorylation, and total tau levels. DMSO, dimethyl sulfoxide. (**B**) Effect of p300 inhibition on SIRT1 levels in control and *TSC1*$^{+/-}$-differentiated SH-SY5Y cells. (**D**) Control and *TSC1*$^{+/-}$ cells were treated for 72 hours with AZD1080 (0.5 μM), a specific phospho-Tau inhibitor. Blots represent the effect of AZD1080 in the phosphorylation status and levels of tau protein. The plot below shows the quantification and statistics of five independent experiments. (**C**) Control and *TSC1*$^{+/-}$ cells were treated with Torin-1. Seventy-two hours later, cells were lysed and the tau acetylation status was assessed by immunoblot. Experiments were performed at least in triplicate. Plots show the means ± SEM for each experiment. Statistical significance was assessed using two-way ANOVA followed by Bonferroni's correction.

and suggested a potential link between *TSC1* insufficiency, tau acetylation, and tauopathies.

DISCUSSION

In the current study, we have validated rare variants in *TSC1* as putative risk alleles for tauopathies; demonstrated the accumulation of acetylated tau in *TSC1*$^{+/-}$ neuronal cells, aging mice, and human brains; and provided a mechanistic basis for tau accumulation in *TSC1* haploinsufficiency (Fig. 9). LOF pathogenic variants in the *TSC1* gene leading to TSC1/hamartin haploinsufficiency have previously been associated with the juvenile-onset lysosomal storage disease TSC (*11*, *41*). In earlier clinical translational studies, we showed a linkage between *TSC1* gene and age-related tauopathies (*10*, *13*). With this study, we have established the mechanistic basis for this linkage, adding *TSC1* to a set of genes including *GBA*, progranulin (*PGRN*), and cathepsin D (*CTSD*) in which pathogenic variants are associated with both childhood developmental and age-associated neurodegenerative diseases (*7*, *8*, *42*). *GBA*, *PGRN*, and *CTSD* genes encode for lysosomal resident proteins and therefore pathogenic variants in these genes lead to disrupted autophagy and lysosome storage disorders (*43*). In contrast, *TSC1* haploinsufficient cells exhibited compensated autophagic flux and prevented tau degradation via aberrant PTMs. Therefore, variants in *TSC1* seemingly represent a related but distinct mechanism for inducing neurodegeneration.

PTMs on tau can markedly affect its function, localization, and degradation. In this study, we demonstrated that TSC1/hamartin insufficiency led to specific tau acetylation and thereby reduced its association with lysosomes, specifically those active for CMA. This finding was supported by a recent report showing that tau hyperacetylation markedly reduces tau degradation through CMA (*28*). While abnormal tau acetylation has been previously described in tauopathies (*3*–*5*, *44*), phosphorylation has historically been considered to be the trigger of tau accumulation and aggregation. In contrast, our study supports acetylation as the key modification leading to tau accumulation through the blockage of its degradation in the lysosomes.

Why tau specifically accumulates in the neurons of tauopathy patients remains unknown. In contrast to other reports, rapamycin treatment did not decrease tau levels in *TSC1*$^{+/-}$ cells. Rapamycin and other rapalogs decrease tau levels by activating macroautophagy

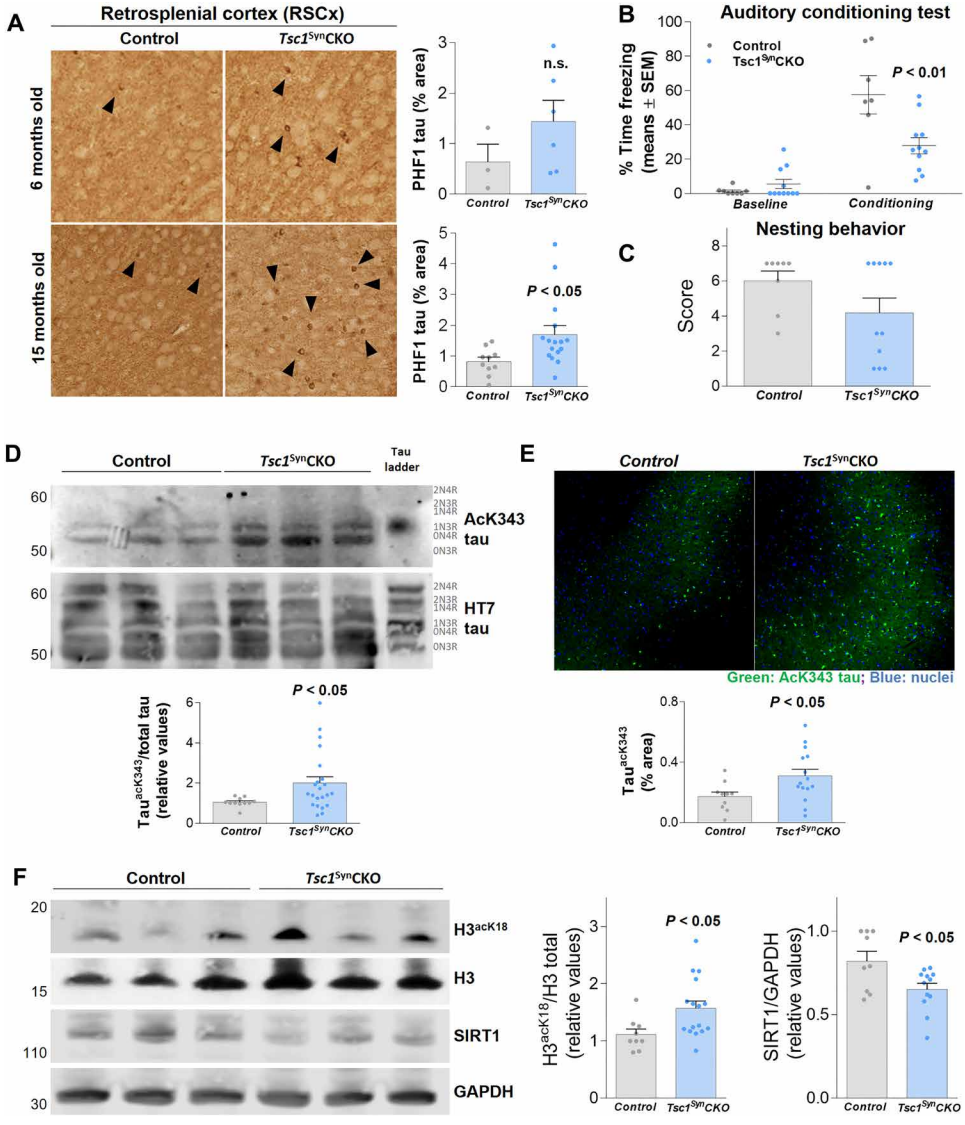

Fig. 7. TSC1/hamartin insufficiency promotes tau acetylation and neurodegeneration in mice. (**A**) PHF1 tau immunostaining performed in the RSCx of *Tsc1*^{Syn1}CKO and control mice, at 6 and 15 months old. Plots represent the percentage of positive tau staining. (**B** and **C**) Auditory conditioning test (B) and nesting behavior score (C) performed in 15-month-old mice. (**D**) Immunoblots showing tau levels, total and acetylated at lysine 343, in the RSCx of 15-month-old mice. The banding pattern was compared to that of the tau ladder, which contains all six recombinant tau isoforms. The HT7 antibody recognized the six tau isoforms whereas the AcK343 antibody only recognized 1N3R and 0N4R isoforms. (**E**) Representative images of the RSCx of 15-month-old mice stained with the AcK343 antibody. The plot represents the means ± SEM of the percentage of the area stained. (**F**) p300 HAT activity, assessed by the acetylation of H3 at K18, and SIRT1 levels were measured in the RSCx of 15-month-old mice. Plots show the means ± SEM of the protein levels. Ten control and 16 *Tsc1*^{Syn1}CKO mice were used for immunostainings/immunoblots. Behavioral tests were performed in 8 control and 11 *Tsc1*^{Syn1}CKO mice. Student's *t* test or two-way ANOVA followed by Bonferroni's correction were used to assess statistical significance.

and thus inducing tau degradation (*45*). However, the accumulation of tau in *TSC1* insufficiency conditions was not due to a macroautophagy failure. Rather, tau accumulation in *TSC1* insufficiency seemed to be the consequence of the specific acetylation of tau that subsequently impaired its degradation by CMA. How TSC1/hamartin regulates tau acetylation and accumulation is not completely unraveled. Here, we showed that *TSC1* insufficiency promoted p300 HAT activity and decreased SIRT1 HDAC levels. In agreement with previous reports (*3*, *31*, *32*), the dysregulation of these enzymes was associated with the specific tau acetylation and accumulation observed under *TSC1* haploinsufficiency conditions. Our results suggested that TSC1/hamartin protein regulated p300 HAT activity through the mTOR pathway. It has been described that mTOR interacts with p300 and regulates its activity (*46*). In *TSC1*$^{+/-}$ cells, the inhibition of mTORC1 and mTORC2 by torin-1 reduced tau levels and acetylation, similar to p300 inhibition. Therefore, the function of TSC1/hamartin as key protein regulating mTOR activity (*16*) could be related with the increased p300 HAT activity and tau acetylation observed in *TSC1* insufficiency. A new function of TSC1/hamartin as co-chaperone for Hsp90 has been reported (*47*). Hsp90

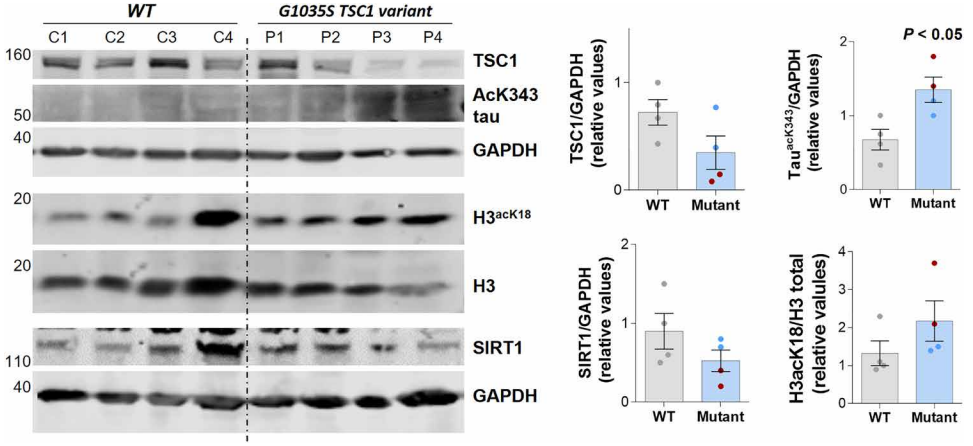

Fig. 8. TSC1/hamartin insufficiency promotes p300/SIRT1 dysregulation and tau acetylation in human brains. Protein was extracted from the inferior frontal cortex of four control subjects (C1 to C4) and four individuals with PSP (P1 to P4). The immunoblots show the protein levels of TSC1 and SIRT1 and the acetylation status of tau. The activity of p300 was measured indirectly by the acetylation status of H3 at K18. GAPDH was used as loading control. The plots show the relative levels of the proteins assessed by immunoblot. P3 and P4 individuals (red dots) exhibited lower levels of TSC1 protein that correlated with increased p300 activity, decreased SIRT1 levels, and increased tau acetylation at K343.

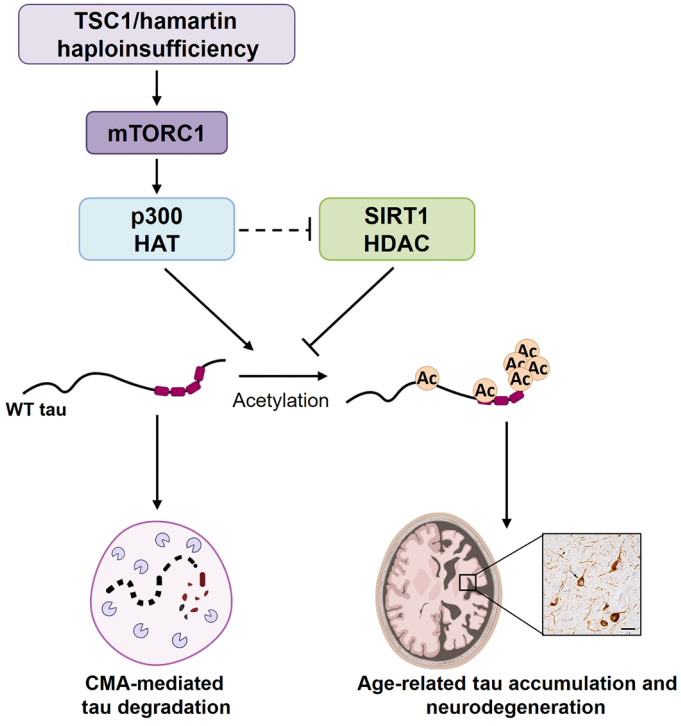

Fig. 9. Proposed model for TSC1/hamartin haploinsufficiency impairing tau degradation and increasing risk for tauopathy. Decreased TSC1/hamartin levels lead to mTORC1 overactivation, which induce the activation of p300 HAT and the decrease of SIRT1 HDAC expression. As a consequence, tau is specifically acetylated at six lysine residues. While WT tau is degraded in the lysosomes through CMA, acetylated tau fails to be degraded by this system and thus accumulates in the neurons, leading to increased risk of neurodegeneration.

seems to be involved with CMA (*48*). Although Hsp90 is not required for targeting of CMA substrates to lysosomes, a fraction of Hsp90 bound at the cytosolic side of the lysosomal membrane contributes to stabilize the binding of CMA substrates once they reach the lysosomal membrane (*49*). Therefore, through its role as co-chaperone for Hsp90, TSC1/hamartin could potentially stabilize the binding of tau to the lysosomes and therefore regulate its degradation via CMA. These two functions of TSC1, regulating tau acetylation and as Hsp90 co-chaperone, could be essential for the specific accumulation of acetylated tau under *TSC1* haploinsufficiency.

Tauopathies are one of the most frequent causes of age-related morbidity; however, no disease-modifying treatments have been generated yet. To develop effective therapies for this diverse group of disorders, the many different etiologies and pathogenic mechanisms must be better understood and appreciated. The lack of models that recapitulate WT, rather than mutant, tau dysfunction has limited our understanding of the molecular mechanisms behind tau accumulation. This distinction is key, as mutant forms of tau can use alternative pathways for clearance as compared to nonmutant tau (*18*, *50*). Thus, models that accumulate nonmutant tau are needed. In this regard, we have developed a powerful genetic model of tauopathy in which human nonmutant hTau accumulated. Although other models of *TSC1* haploinsufficiency were previously generated, most of them have been used to study neuronal development and clinical TSC (*51*–*53*), but not age-related neurodegenerative diseases.

TSC1 haploinsufficiency induced the accumulation of nonmutant tau protein in cultured neurons as well as in mice and human brains. However, our results did not clarify how exactly the loss of TSC1/hamartin led to the specific accumulation of tau rather than TDP-43 or other neurodegenerative disease proteins (*10*). Although the unanswered question of specificity represents a limitation of this study, the selective neuronal vulnerability to different neurodegenerative disease proteins remains unknown throughout the field. *TSC1* insufficient cell lines and mice may provide new models in which to address this highly important and compelling issue.

Here, we have established a mechanistic link between TSC1/hamartin protein, tau acetylation, and tau accumulation. Blocking acetylation with a specific p300 HAT inhibitor or promoting deacetylation with a SIRT1 HDAC activator normalized tau levels in *TSC1* insufficiency conditions. Other studies have shown that the dysregulation of both enzymes is involved in tau acetylation and neurodegeneration

(*3*, *31*, *32*). In addition, several clinical trials are currently investigating the neuroprotective effect of the pharmacological modulation of p300 and SIRT1 (*54*, *55*). This study supports the translation of p300 and SIRT1 into targets for drug development for the treatment of tauopathies. Furthermore, the identified tau acetyl-lysine residues could represent biomarkers for tauopathy diagnosis and progression. Last, the novel cellular and animal models of nonmutant tau accumulation that we have generated could be used as preclinical models to develop disease-modifying treatments, potentially facilitating the successful translation of future therapies to humans.

METHODS

Human genetics and postmortem brain lysates

In the genetic analysis, two cohorts of tauopathy patients (EOAD, n = 228; and PSP, n = 501) were analyzed for the presence of rare *TSC1* variants. *TSC1* variant calls were verified via Sanger sequencing. The allele frequency of rare *TSC1* variants in the EOAD and PSP cohort was compared with the allele frequency of these variants in non–Finnish European controls from the Genome Aggregation Database (gnomAD v2.1.1; https://gnomad.broadinstitute.org/variant/9-135771987-C-CGCT?dataset=gnomad_r2_1) and the ADSP Discovery Case Control database (www.niagads.org/sites/all/public_files/ADSP%20%20SUMMARY%20PLAN%20revised%20fnl%2041513.pdf), respectively. A detailed explanation of the methodology used to study the enrichment of *TSC1* variants in tauopathy cases is included as supplementary material.

Postmortem tissue from four healthy control individuals and four individuals from the PSP cohort carrying the G1035S variant in *TSC1* was obtained from Mayo Clinic (Jacksonville, FL). Total protein was extracted from the inferior frontal cortex using radioimmunoprecipitation assay (RIPA) buffer. Then, protein levels were assessed by immunoblot. The demographics of the individuals used in this studio is shown in table S1. All the participants of this study or their surrogates provided written informed consent to participate in this study, and the institutional review boards at each site approved all aspects of the study.

Culture and generation of stable SH-SY5Y cell lines

SH-SY5Y neuroblastoma cells (American Type Culture Collection, #CRL-2266) were cultured in Eagle's Minimum Essential Medium (EMEM):F12 medium supplemented with 10% (v/v) heat-inactivated fetal bovine serum (FBS) and 1% penicillin/streptomycin (P/S). *TSC1* heterozygous SH-SY5Y cell lines (*TSC1*$^{+/-}$) were generated using the CRISPR-Cas9 system as previously described (*10*). *TSC2* knockdown stable cell lines were generated by infecting SH-SY5Y cells with tuberin short hairpin RNA (h) lentiviral particles (Santa Cruz Biotechnology, #sc-36762-V) followed by puromycin selection (1 μg/ml). To generate stable SH-SY5Y cell lines overexpressing TSC1/hamartin (WT and mutant) and 2N4R tau (WT, acetyl-mimetic K➔Q and non-acetylatable K➔R), we cloned WT and mutant forms of the *TSC1* and *MAPT*/tau genes in the pLenti-CMV plasmid (Addgene plasmid #17392) (*56*). Lentiviral particles were generated in HEK293FT cells and used to transduce SH-SY5Y cells as previously described (*10*). Cells expressing the plasmids were selected with neomycin (2 μg/μl), expanded, and banked. Overexpressed proteins were tagged with myc (N-terminal) and FLAG (C-terminal) tags. Efficiency of protein overexpression was assessed by immunoblotting with antibodies against the myc and FLAG tags.

Generation and culture of the fibroblast lines

Epithelial fibroblast cells were obtained from the Memory and Aging Center Fibroblast Bank at the University of California, San Francisco. The skin biopsy was performed after obtaining the donor's written informed consent. The consent allowed for use of tissue by all parties, commercial and academic, for the purposes of research but not for use in human therapy. The informed consent and the protocol of our study were approved by the UCSF Institutional Review Board and Ethics Committee. The biopsy tissue was placed into a tissue culture dish with a coverslip on top. Fibroblasts were fed every 2 to 3 days with Dulbecco's modified Eagle's medium (Thermo Fisher Scientific, #11995073) supplemented with 10% (v/v) heat-inactivated FBS and 1% P/S. Cells were expanded, tested negative for mycoplasma, banked, and used in further experiments.

iPSC line generation, genome engineering, and characterization

The TSC1-family iPSC lines were generated from epithelial fibroblasts from each member of the family, including three *TSC1* mutation carriers and one nonmutation carrier that was used as a control (table S2). For additional control lines, we used two well-characterized WT iPSC lines: the F11350 iPSC line obtained from the Karch laboratory at Washington University School of Medicine (*57*) and the PGP-1 iPSC line (GM23338) derived from a 55-year-old male obtained from the Coriell Institute for Medical Research (table S2).

Two monoclonal *TSC1*$^{+/-}$ iPSC lines were generated by the company Synthego in the background of the WT PGP-1 iPSC using the CRISPR-Cas9 gene editing system. Briefly, an single guide RNA (5′-ACCAAGGUGUUUACAAGCAU-3′) targeting the *TSC1 gene* was designed and validated before the nucleofection of iPSC, as previously described (*58*). To select *TSC1*$^{+/-}$ iPSC clones, genomic DNA was extracted with the QuickExtract Kit (Epicentre, #QE09050). PCR was performed using Q5 Hot Start High-Fidelity 2X Master Mix, using 5′-GCAGAACTGTAATGCTGCACAA-3′ and 5′-TCAAGAATCATGGGTCCTACAAAGT-3′ primers. The PCR program was 98°C for 30 s, 30 cycles of 98°C for 10 s, 66°C for 30 s, and 72°C for 25 s, and a final stage at 72°C for 10 min. Two *TSC1* heterozygous (*TSC1*$^{+/-}$) CRISPR lines (B02 and C10) were identified, expanded, and banked.

After the generation, both TSC1-family and CRISPR-engineered iPSC lines were verified for the expression of pluripotency markers (SSEA4, Oct4, and SOX2) by immunofluorescence as previously described (figs. S1 and S2) (*57*). In addition, chromosomal abnormalities in all iPSC lines were assessed by G-band karyotyping using standard cytogenetic procedures (figs. S1 and S2).

All iPSC lines were maintained in Matrigel (Corning, #354277)–coated plates using mTSER media (STEMCELL Technologies, #05850). For passaging, iPSCs were detached using Accutase (Thermo Fisher Scientific, #A1110501) and seeded using mTSER media supplemented with 10 μM Rock inhibitor (Y-27632, STEMCELL Technologies, #72304). Media was replaced every day.

SH-SY5Y and iPSC differentiation into neurons

For the neuronal differentiation of SH-SY5Y cells, 10,000 cells/cm^2 were seeded in tissue culture plates 24 hours before starting the differentiation through the addition of 10 μM retinoic acid (RA) in EMEM/F12 media supplemented with 10% FBS and 1% P/S. After 6 days of RA treatment, cells were treated for 4 days with brain-derived neurotrophic factor (50 ng/ml) in EMEM/F12 media supplemented only with 1% P/S (*58*). Human iPSCs were differentiated into cortical

neurons by infection with virus particles containing doxycycline-inducible neurogenin-2 (Ngn2) and puromycin resistance as previously described (*58*, *59*). After infection, cells were cultured for 21 days before lysate collection.

Whole-cell lysates and lysosome isolation

For whole lysates, cells were harvested and lysed with Pierce RIPA buffer [25 mM tris-HCl (pH 7.6), 150 mM NaCl, 1% NP-40, 1% sodium deoxycholate, and 0.1% SDS; Thermo Fisher Scientific, #89900] containing protease (MilliporeSigma, #4693124001), phosphatase (MilliporeSigma, #4906837001), and deacetylase inhibitors 3 μM trichostatin A (Cayman Chemical Company, #89730) and 10 mM niacinamide (MilliporeSigma, #N5535). Then, lysates were centrifuged at 15,000 rpm for 15 min at 4°C to obtain the supernatant containing soluble proteins.

Lysosomes were isolated from differentiated SH-SY5Y cells following a protocol previously published (*25*). Briefly, 40 million differentiated SH-SY5Y cells were collected and lysed in 0.25 M sucrose buffer. After serial centrifugations, a fraction containing both mitochondria and lysosomes was obtained. Lysosomes were isolated and separated from the mitochondrial fraction in a discontinuous density gradient. After centrifugation, lysosomes appear in two aqueous density-dependent layers, and the less dense fraction containing CMA^+ lysosomes and the denser fraction containing a combination of CMA^+ and CMA^- lysosomes further separated by differential centrifugation. Lysosomal fractions were resuspended in 0.3 M sucrose and centrifuged again at 10,000*g* for 5 min. Pellets containing the two lysosome fractions were then diluted in 0.25 M sucrose buffer before analysis.

Generation of anti-tau acetyl lysine 343 antibody, Western blotting, and protein half-life measurement

Monoclonal anti-tau acetyl lysine 343 (AcK343) antibody was generated in the antibody development facility of Fred Hutchinson Cancer Research Center (Seattle, WA). Mice were immunized using the peptide sequence CVEVKSE(KAc)LDFKD, containing the K343 residue of 2N4R tau. Site specificity of AcK343 was confirmed using acetylated and non-acetylated forms of tau peptides that bind to bovine serum albumin (BSA) protein (fig. S15).

For Western blotting, equivalent amounts of protein were separated on a 4 to 12% bis-tris gel (Thermo Fisher Scientific). Immunoblotting was performed as previously described (*58*) using the antibodies listed in the Supplementary Materials (table S3). Immunoreactive bands were visualized using the LI-COR Odyssey CLx imaging system and quantified using the ImageJ software.

To measure the half-life of WT and mutant TSC1/hamartin protein, SH-SY5Y cells expressing FLAG-tagged WT or mutant TSC1/hamartin were seeded into six-well plates at 1×10^6 cells per well. Twenty-four hours after seeding, cells were treated with CHX (50 μg/ml) and lysates were collected at 0, 8, 24, 48, and 72 hours into cold RIPA buffer. Degradation of FLAG-tagged TSC1/hamartin protein was evaluated by immunoblot with an anti-FLAG antibody. Protein half-life was calculated with the following equation: Half-life ($T_{1/2}$) = ln(2)/K, where K = degradation rate constant ($hour^{-1}$).

Immunoprecipitation and mass spectrometry

Endogenous tau was immunoprecipitated from whole lysates of differentiated SH-SY5Y cells (1 mg) using 10 μg of the HT7 tau antibody (Thermo Fisher Scientific, #MN1000) and the cross-link magnetic immunoprecipitation kit (Thermo-Pierce, #PI88805) following the manufacturer's instructions. Immunoprecipitated proteins were separated on a 4 to 12% bis-tris gel and stained with SafeStain (Thermo Fisher Scientific, #LC6060). A broad band around 50 kDa was cut out from the gel, digested with trypsin, and analyzed by mass spectrometry. The identification of peptides and PTMs in tau-enriched samples was performed at the UCSF Mass Spectrometry Facility following standard protocols (*60*, *61*).

qPCR analysis

SH-SY5Y cells were differentiated in 10-cm plates and either collected right after differentiation or treated with A485 (15 μM) or dimethyl sulfoxide for 72 hours before collection. mRNA was extracted using the RNeasy Kit (Qiagen, #217004) per the manufacturer's protocol. Extracted mRNA was converted to cDNA by PCR using SuperScript III Reverse Transcriptase (Invitrogen, #18080-044). The expression of the *MAPT*/tau gene and *SIRT1* gene was measured by qPCR using standard techniques as previously described (*58*). *GAPDH* and *actin* were used as controls.

Autophagy analysis

Measurement of macroautophagy in differentiated SH-SY5Y cells was performed as previously described (*22*). Briefly, cells were treated with the V-ATPase inhibitor bafilomycin A1 (BafA1; 100 nM) for 6 hours to block protein degradation in the lysosomes, lysates were collected, and then LC3-II protein levels were assessed by immunoblot. An increase in LC3-II levels after BafA1 treatment corresponds to an increase in autophagy flux.

Macroautophagy activity in fibroblasts was measured after transduction with lentivirus carrying an mCherry-GFP-LC3 tandem construct (*20*). Fibroblasts were plated on glass-bottom 96-well plates and fixed with 4% paraformaldehyde (PFA), and fluorescence was read in both red and green channels using high-content microscopy (Operetta, PerkinElmer). Images of nine different fields per well were captured, resulting in an average of 2500 to 3000 cells per view. The number of particles/puncta per cell was quantified using the "particle identifier" function in the cytosolic region (*62*). Values were presented as number of puncta per cell section. Positive puncta for both fluorophores correspond to autophagosomes, whereas those only positive for the red fluorophore correspond to autolysosomes. Autophagic flux was determined as the conversion of autophagosomes (yellow) to autolysosomes (red-only puncta) (*20*).

Immunofluorescence, confocal laser scanning microscopy, and colocalization analysis

Undifferentiated and differentiated SH-SY5Y cells were seeded in microscopy chambers (Thermo Fisher Scientific, #155382). When confluent, cells were fixed for 30 min in 4% PFA in phosphate-buffered saline (PBS). Then, cells were washed twice with glycine (2 mg/ml) and blocked with 2% BSA in PBS for 1 hour. Cells were permeabilized with 0.1% saponin, incubated with primary antibodies for 1 hour at room temperature, and then incubated with the corresponding secondary antibodies for 45 min at room temperature. ProLong Gold Antifade Reagent with 4′,6-diamidino-2-phenylindole was used for nuclear staining (Cell Signaling Technology, #8961S). Stains were visualized in the High Speed Widefield confocal (UCSF Nikon core) using a water immersion 63× objective using green fluorescein isothiocyanate–488 excitation and far-red 647 excitation. Pearson's correlation coefficient measured with Fiji/ImageJ was used to estimate the colocalization between both channels.

Measurement of p300 HAT activity

The acetyl transferase activity of p300 was measured using the HAT activity colorimetric assay kit (MilliporeSigma, #EPI001) per the manufacturer's instructions. Briefly, differentiated SH-SY5Y cells were collected and washed with PBS, and proteins were extracted with CHAPS buffer [50 mM Hepes (pH 7.4), 40 mM NaCl, 2 mM EDTA, 1 mM orthovanadate, 50 mM NaF, 10 mM pyrophosphate, and 0.3% CHAPS] including protease and phosphatase inhibitors. Then, 75 μg of whole lysate was incubated with the kit assay mix and run in triplicate in 96-well plates for 1 hour at 37°C. Values were read at an optical density of 440 nm using the Tecan M200 Pro plate reader. To block the activity of p300 HAT, lysates were treated for 30 min at 37°C with the specific p300 inhibitor, A485. The activity of p300 HAT was assessed by subtracting the remaining HAT activity after A485 treatment from the initial values in nontreated lysates.

Transgenic mouse generation and brain lysates extraction

hTau;TSC1$^{Syn1+/+}$ and *hTau;TSC1*$^{Syn1+/-}$ transgenic mice were bred and maintained in-house at Washington University in St. Louis School of Medicine. hTau mice hemizygous (Cre+ or *hTau;TSC1*$^{Syn1+/-}$) or homozygous (Cre– or *hTau;TSC1*$^{Syn1+/+}$) for TSC1 were age-matched and randomized across both sex and litter for use in studies at either 6 months old ($n = 3$ *hTau;TSC1*$^{Syn1+/+}$ and $n = 6$ *hTau;TSC1*$^{Syn1+/-}$) or 15 months old ($n = 10$ *hTau;TSC1*$^{Syn1+/+}$ and $n = 16$ *hTau;TSC1*$^{Syn1+/-}$). Methodology for the generation of transgenic mice, behavior analysis, euthanasia, tissue processing, immunohistochemistry, imaging, and quantification is included as supplementary material.

For protein quantification studies, the RSCx was isolated and lysed by mechanical disruption in cold RIPA buffer. Then, the fraction containing soluble proteins was extracted by centrifugation at 15,000 rpm at 4°C for 15 min. To concentrate tau protein, 20 μl of the resultant supernatant was heated at 95°C for 30 min. After the heat shock, samples were centrifuged again at 15,000 rpm at 4°C for 20 min. The supernatant corresponding to the heat stable fraction, which mostly contains tau protein, was collected and analyzed by immunoblot. For tau fractionation experiments, brain tissue was lysed in RAB buffer, RIPA buffer, and 70% formic acid as previously described (*40*).

Statistical analysis

Student's *t* test and one-way and two-way analysis of variance (ANOVA) statistical analyses were performed using GraphPad Prism 6. Bonferroni's analysis was performed to analyze the statistical significance between multiple groups. Plots show means ± SEM and *P* values for all the experiments performed. Differences were considered statistically significant when $P < 0.05$.

SUPPLEMENTARY MATERIALS

Supplementary material for this article is available at https://science.org/doi/10.1126/sciadv.abg3897

View/request a protocol for this paper from *Bio-protocol*.

REFERENCES AND NOTES

1. T. Revesz, J. L. Holton, Anatamopathological spectrum of tauopathies. *Mov. Disord.* **18**, 13–20 (2003).
2. D. Vilchez, I. Saez, A. Dillin, The role of protein clearance mechanisms in organismal ageing and age-related diseases. *Nat. Commun.* **5**, 1–13 (2014).
3. S. W. Min, S. H. Cho, Y. Zhou, S. Schroeder, V. Haroutunian, W. W. Seeley, E. J. Huang, Y. Shen, E. Masliah, C. Mukherjee, D. Meyers, P. A. Cole, M. Ott, L. Gan, Acetylation of tau inhibits its degradation and contributes to tauopathy. *Neuron* **67**, 953–966 (2010).
4. T. J. Cohen, J. L. Guo, D. E. Hurtado, L. K. Kwong, I. P. Mills, J. Q. Trojanowski, V. M. Y. Lee, The acetylation of tau inhibits its function and promotes pathological tau aggregation. *Nat. Commun.* **2**, 252 (2011).
5. C. Alquezar, S. Arya, A. W. Y. Kao, Tau post-translational modifications: Dynamic transformers of tau function, degradation, and aggregation. *Front. Neurol.* **11**, 1826 (2020).
6. J. Aharon-Peretz, H. Rosenbaum, R. Gershoni-Baruch, Mutations in the glucocerebrosidase gene and Parkinson's disease in Ashkenazi Jews. *N. Engl. J. Med.* **351**, 1972–1977 (2004).
7. E. Sidransky, G. Lopez, The link between the GBA gene and parkinsonism. *Lancet Neurol.* **11**, 986–998 (2012).
8. S. Ketterer, A. Gomez-Auli, L. E. Hillebrand, A. Petrera, A. Ketscher, T. Reinheckel, Inherited diseases caused by mutations in cathepsin protease genes. *FEBS J.* **284**, 1437–1454 (2017).
9. M. Baker, I. R. Mackenzie, S. M. Pickering-Brown, J. Gass, R. Rademakers, C. Lindholm, J. Snowden, J. Adamson, A. D. Sadovnick, S. Rollinson, A. Cannon, E. Dwosh, D. Neary, S. Melquist, A. Richardson, D. Dickson, Z. Berger, J. Eriksen, T. Robinson, C. Zehr, C. A. Dickey, R. Crook, E. McGowan, D. Mann, B. Boeve, H. Feldman, M. Hutton, Mutations in progranulin cause tau-negative frontotemporal dementia linked to chromosome 17. *Nature* **442**, 916–919 (2006).
10. N. T. Olney, C. Alquezar, E. M. Ramos, A. L. Nana, J. C. Fong, A. M. Karydas, J. B. Taylor, M. L. Stephens, A. R. Argouarch, V. A. Van Berlo, D. R. Dokuru, E. H. Sherr, G. A. Jicha, W. P. Dillon, R. S. Desikan, M. De May, W. W. Seeley, G. Coppola, B. L. Miller, A. W. Kao, Linking tuberous sclerosis complex, excessive mTOR signaling, and age-related neurodegeneration: A new association between TSC1 mutation and frontotemporal dementia. *Acta Neuropathol.* **134**, 813–816 (2017).
11. D. M. Hasbani, P. B. Crino, in *Handbook of Clinical Neurology* (Elsevier B.V., 2018), vol. 148, pp. 813–822.
12. E. P. Henske, S. Józwiak, J. C. Kingswood, J. R. Sampson, E. A. Thiele, Tuberous sclerosis complex. *Nat. Rev. Dis. Prim.* **2**, 1–18 (2016).
13. A. J. Liu, A. M. Staffaroni, J. C. Rojas-Martinez, N. T. Olney, C. Alquezar-Burillo, P. A. Ljubenkov, R. La Joie, J. C. Fong, J. Taylor, A. Karydas, E. M. Ramos, G. Coppola, A. L. Boxer, G. D. Rabinovici, B. L. Miller, A. W. Kao, Association of cognitive and behavioral features between adults with tuberous sclerosis and frontotemporal dementia. *JAMA Neurol.* **77**, 358–366 (2020).
14. J. N. Cochran, E. G. Geier, L. W. Bonham, J. S. Newberry, M. D. Amaral, M. L. Thompson, B. N. Lasseigne, A. M. Karydas, E. D. Roberson, G. M. Cooper, G. D. Rabinovici, B. L. Miller, R. M. Myers, J. S. Yokoyama, Non-coding and loss-of-function coding variants in TET2 are associated with multiple neurodegenerative diseases. *Am. J. Hum. Genet.* **106**, 632–645 (2020).
15. S. Rogers, R. Wells, M. Rechsteiner, Amino acid sequences common to rapidly degraded proteins: The PEST hypothesis. *Science* **234**, 364–368 (1986).
16. A. R. Tee, D. C. Fingar, B. D. Manning, D. J. Kwiatkowski, L. C. Cantley, J. Blenis, Tuberous sclerosis complex-1 and -2 gene products function together to inhibit mammalian target of rapamycin (mTOR)-mediated downstream signaling. *Proc. Natl. Acad. Sci. U.S.A.* **99**, 13571–13576 (2002).
17. M. Laplante, D. M. Sabatini, mTOR signaling in growth control and disease. *Cell* **149**, 274–293 (2012).
18. B. Caballero, Y. Wang, A. Diaz, I. Tasset, Y. R. Juste, B. Stiller, E.-M. E. E. M. Mandelkow, E.-M. E. E. M. Mandelkow, A. M. Cuervo, Interplay of pathogenic forms of human tau with different autophagic pathways. *Aging Cell* **17**, e12692 (2018).
19. Y. Wang, M. Martinez-Vicente, U. Krüger, S. Kaushik, E. Wong, E.-M. Mandelkow, A. M. Cuervo, E. Mandelkow, Tau fragmentation, aggregation and clearance: The dual role of lysosomal processing. *Hum. Mol. Genet.* **18**, 4153–4170 (2009).
20. S. Kimura, T. Noda, T. Yoshimori, Dissection of the autophagosome maturation process by a novel reporter protein, tandem fluorescent-tagged LC3. *Autophagy* **3**, 452–460 (2007).
21. M. Bordi, M. J. Berg, P. S. Mohan, C. M. Peterhoff, M. J. Alldred, S. Che, S. D. Ginsberg, R. A. Nixon, Autophagy flux in CA1 neurons of Alzheimer hippocampus: Increased induction overburdens failing lysosomes to propel neuritic dystrophy. *Autophagy* **12**, 2467–2483 (2016).
22. S. R. Yoshii, N. Mizushima, Monitoring and measuring autophagy. *Int. J. Mol. Sci.* **18**, 1865 (2017).
23. A. Caccamo, A. Magrì, D. X. Medina, E. V. Wisely, M. F. López-Aranda, A. J. Silva, S. Oddo, mTOR regulates tau phosphorylation and degradation: Implications for Alzheimer's disease and other tauopathies. *Aging Cell* **12**, 370–380 (2013).
24. U. Bandyopadhyay, S. Sridhar, S. Kaushik, R. Kiffin, A. M. Cuervo, Identification of regulators of chaperone-mediated autophagy. *Mol. Cell* **39**, 535–547 (2010).
25. A. M. Cuervo, J. F. Dice, E. Knecht, A population of rat liver lysosomes responsible for the selective uptake and degradation of cytosolic proteins. *J. Biol. Chem.* **272**, 5606–5615 (1997).
26. A. E. Majeski, J. Fred Dice, Mechanisms of chaperone-mediated autophagy. *Int. J. Biochem. Cell Biol.* **36**, 2435–2444 (2004).
27. T. J. Cohen, A. W. Hwang, C. R. Restrepo, C. X. Yuan, J. Q. Trojanowski, V. M. Y. Lee, An acetylation switch controls TDP-43 function and aggregation propensity. *Nat. Commun.* **6**, 5845 (2015).

28. B. Caballero, M. Bourdenx, E. Luengo, A. Diaz, P. D. Sohn, X. Chen, C. Wang, Y. R. Juste, S. Wegmann, B. Patel, Z. T. Young, S. Y. Kuo, J. A. Rodriguez-Navarro, H. Shao, M. G. Lopez, C. M. Karch, A. M. Goate, J. E. Gestwicki, B. T. Hyman, L. Gan, A. M. Cuervo, Acetylated tau inhibits chaperone-mediated autophagy and promotes tau pathology propagation in mice. *Nat. Commun.* **12**, 2238 (2021).
29. Y. Carlomagno, D.-E. C. Chung, M. Yue, M. Castanedes-Casey, B. J. Madden, J. Dunmore, J. Tong, M. DeTure, D. W. Dickson, L. Petrucelli, C. Cook, An acetylation–phosphorylation switch that regulates tau aggregation propensity and function. *J. Biol. Chem.* **292**, 15277–15286 (2017).
30. D. Ajit, H. Trzeciakiewicz, J. H. Tseng, C. M. Wander, Y. Chen, A. Ajit, D. P. King, T. J. Cohen, A unique tau conformation generated by an acetylation-mimic substitution modulates P301S-dependent tau pathology and hyperphosphorylation. *J. Biol. Chem.* **294**, 16698–16711 (2019).
31. S.-W. Min, X. Chen, T. E. Tracy, Y. Li, Y. Zhou, C. Wang, K. Shirakawa, S. S. Minami, E. Defensor, S. A. Mok, P. D. Sohn, B. Schilling, X. Cong, L. Ellerby, B. W. Gibson, J. Johnson, N. Krogan, M. Shamloo, J. Gestwicki, E. Masliah, E. Verdin, L. Gan, Critical role of acetylation in tau-mediated neurodegeneration and cognitive deficits. *Nat. Med.* **21**, 1154–1162 (2015).
32. S. W. Min, P. D. Sohn, Y. Li, N. Devidze, J. R. Johnson, N. J. Krogan, E. Masliah, S. A. Mok, J. E. Gestwicki, L. Gan, SIRT1 deacetylates tau and reduces pathogenic tau spread in a mouse model of tauopathy. *J. Neurosci.* **38**, 3680–3688 (2018).
33. K. J. Janczura, C. H. Volmar, G. C. Sartor, S. J. Rao, N. R. Ricciardi, G. Lambert, S. P. Brothers, C. Wahlestedt, Inhibition of HDAC3 reverses Alzheimer's disease-related pathologies in vitro and in the 3xTg-AD mouse model. *Proc. Natl. Acad. Sci. U.S.A.* **115**, E11148–E11157 (2018).
34. L. M. Lasko, C. G. Jakob, R. P. Edalji, W. Qiu, D. Montgomery, E. L. Digiammarino, T. M. Hansen, R. M. Risi, R. Frey, V. Manaves, B. Shaw, M. Algire, P. Hessler, L. T. Lam, T. Uziel, E. Faivre, D. Ferguson, F. G. Buchanan, R. L. Martin, M. Torrent, G. G. Chiang, K. Karukurichi, J. W. Langston, B. T. Weinert, C. Choudhary, P. De Vries, J. H. Van Drie, D. McElligott, E. Kesicki, R. Marmorstein, C. Sun, P. A. Cole, S. H. Rosenberg, M. R. Michaelides, A. Lai, K. D. Bromberg, Discovery of a selective catalytic p300/CBP inhibitor that targets lineage-specific tumours. *Nature* **550**, 128–132 (2017).
35. A. K. Singh, A. Bishayee, A. K. Pandey, Targeting histone deacetylases with natural and synthetic agents: An emerging anticancer strategy. *Nutrients* **10**, 731 (2018).
36. M. M. Milczarek, S. D. Vann, F. Sengpiel, Spatial memory engram in the mouse retrosplenial cortex. *Curr. Biol.* **28**, 1975–1980.e6 (2018).
37. E. L. Hindley, A. J. D. Nelson, J. P. Aggleton, S. D. Vann, Dysgranular retrosplenial cortex lesions in rats disrupt cross-modal object recognition. *Learn. Mem.* **21**, 171–179 (2014).
38. P. J. Nestor, T. D. Fryer, M. Ikeda, J. R. Hodges, Retrosplenial cortex (BA 29/30) hypometabolism in mild cognitive impairment (prodromal Alzheimer's disease). *Eur. J. Neurosci.* **18**, 2663–2667 (2003).
39. N. M. Weinberger, Auditory associative memory and representational plasticity in the primary auditory cortex. *Hear. Res.* **229**, 54–68 (2007).
40. K. M. M. Schoch, S. L. L. DeVos, R. L. L. Miller, S. J. J. Chun, M. Norrbom, D. F. F. Wozniak, H. N. N. Dawson, C. F. Bennett, F. Rigo, T. M. M. Miller, Increased 4R-tau induces pathological changes in a human-tau mouse model. *Neuron* **90**, 941–947 (2016).
41. F. J. DiMario, M. Sahin, D. Ebrahimi-Fakhari, Tuberous sclerosis complex. *Pediatr. Clin. North Am.* **62**, 633–648 (2015).
42. A. E. Arrant, V. C. Onyilo, D. E. Unger, E. D. Roberson, Progranulin gene therapy improves lysosomal dysfunction and microglial pathology associated with frontotemporal dementia and neuronal ceroid lipofuscinosis. *J. Neurosci.* **38**, 2341–2358 (2018).
43. F. M. Platt, A. d'Azzo, B. L. Davidson, E. F. Neufeld, C. J. Tifft, Lysosomal storage diseases. *Nat. Rev. Dis. Prim.* **4**, 1–25 (2018).
44. C. Cook, J. N. Stankowski, Y. Carlomagno, C. Stetler, L. Petrucelli, Acetylation: A new key to unlock tau's role in neurodegeneration. *Alzheimer's Res. Ther.* **6**, 29 (2014).
45. M. C. Silva, G. A. Nandi, S. Tentarelli, I. K. Gurrell, T. Jamier, D. Lucente, B. C. Dickerson, D. G. Brown, N. J. Brandon, S. J. Haggarty, Prolonged tau clearance and stress vulnerability rescue by pharmacological activation of autophagy in tauopathy neurons. *Nat. Commun.* **11**, 3258 (2020).
46. W. Wan, Z. You, Y. Xu, L. Zhou, Z. Guan, C. Peng, C. C. L. Wong, H. Su, T. Zhou, H. Xia, W. Liu, mTORC1 phosphorylates acetyltransferase p300 to regulate autophagy and lipogenesis. *Mol. Cell.* **68**, 323–335.e6 (2017).
47. C. A. Dickey, A. Kamal, K. Lundgren, N. Klosak, R. M. Bailey, J. Dunmore, P. Ash, S. Shoraka, J. Zlatkovic, C. B. Eckman, C. Patterson, D. W. Dickson, N. S. Nahman, M. Hutton, F. Burrows, L. Petrucelli, The high-affinity HSP90-CHIP complex recognizes and selectively degrades phosphorylated tau client proteins. *J. Clin. Invest.* **117**, 648–658 (2007).
48. U. Bandyopadhyay, S. Kaushik, L. Varticovski, A. M. Cuervo, The chaperone-mediated autophagy receptor organizes in dynamic protein complexes at the lysosomal membrane. *Mol. Cell. Biol.* **28**, 5747–5763 (2008).
49. Z. Gong, I. Tasset, A. Diaz, J. Anguiano, E. Tas, L. Cui, R. Kuliawat, H. Liu, B. Kühn, A. M. Cuervo, R. Muzumdar, Humanin is an endogenous activator of chaperone-mediated autophagy. *J. Cell Biol.* **217**, 635–647 (2018).
50. V. A. Polito, H. Li, H. Martini-Stoica, B. Wang, L. Yang, Y. Xu, D. B. Swartzlander, M. Palmieri, A. Ronza, V. M. Lee, M. Sardiello, A. Ballabio, H. Zheng, Selective clearance of aberrant tau proteins and rescue of neurotoxicity by transcription factor EB. *EMBO Mol. Med.* **6**, 1142–1160 (2014).
51. A. G. Nadadhur, M. Alsaqati, L. Gasparotto, P. Cornelissen-Steijger, E. van Hugte, S. Dooves, A. J. Harwood, V. M. Heine, Neuron-glia interactions increase neuronal phenotypes in tuberous sclerosis complex patient ipsc-derived models. *Stem Cell Rep.* **12**, 42–56 (2019).
52. W. Afshar Saber, M. Sahin, Recent advances in human stem cell-based modeling of tuberous sclerosis complex. *Mol. Autism.* **11**, 16 (2020).
53. J. D. Blair, D. Hockemeyer, H. S. Bateup, Genetically engineered human cortical spheroid models of tuberous sclerosis. *Nat. Med.* **24**, 1568–1578 (2018).
54. R. S. Turner, R. G. Thomas, S. Craft, C. H. Van Dyck, J. Mintzer, B. A. Reynolds, J. B. Brewer, R. A. Rissman, R. Raman, P. S. Aisen, A randomized, double-blind, placebo-controlled trial of resveratrol for Alzheimer disease. *Neurology* **85**, 1383–1391 (2015).
55. L. VandeVrede, M. L. Dale, S. Fields, M. Frank, E. Hare, H. W. Heuer, K. Keith, M. Koestler, P. A. Ljubenkov, D. McDermott, N. Ohanesian, J. Richards, J. C. Rojas, E. H. Thijssen, C. Walsh, P. Wang, A. Wolf, J. F. Quinn, R. Tsai, A. L. Boxer, Open-label phase 1 futility studies of salsalate and young plasma in progressive supranuclear palsy. *Mov. Disord. Clin. Pract.* **7**, 440–447 (2020).
56. E. Campeau, V. E. Ruhl, F. Rodier, C. L. Smith, B. L. Rahmberg, J. O. Fuss, J. Campisi, P. Yaswen, P. K. Cooper, P. D. Kaufman, A versatile viral system for expression and depletion of proteins in mammalian cells. *PLOS ONE* **4**, e6529 (2009).
57. C. M. Karch, A. W. Kao, A. Karydas, K. Onanuga, R. Martinez, A. Argouarch, C. Wang, C. Huang, P. D. Sohn, K. R. Bowles, S. Spina, M. C. Silva, J. A. Marsh, S. Hsu, D. A. Pugh, N. Ghoshal, J. Norton, Y. Huang, S. E. Lee, W. W. Seeley, P. Theofilas, L. T. Grinberg, F. Moreno, K. McIlroy, B. F. Boeve, N. J. Cairns, J. F. Crary, S. J. Haggarty, J. K. Ichida, K. S. Kosik, B. L. Miller, L. Gan, A. M. Goate, S. Temple, C. Alquezar, K. Bowles, D. Butler, I. Hernandez, V. Hennes, M. Kampmann, A comprehensive resource for induced pluripotent stem cells from patients with primary tauopathies. *Stem Cell Rep.* **13**, 939–955 (2019).
58. C. Alquezar, J. B. Felix, E. McCandlish, B. T. Buckley, D. Caparros-Lefebvre, C. M. Karch, L. I. Golbe, A. W. Kao, Heavy metals contaminating the environment of a progressive supranuclear palsy cluster induce tau accumulation and cell death in cultured neurons. *Sci. Rep.* **10**, 569 (2020).
59. Y. Zhang, C. Pak, Y. Han, H. Ahlenius, Z. Zhang, S. Chanda, S. Marro, C. Patzke, C. Acuna, J. Covy, W. Xu, N. Yang, T. Danko, L. Chen, M. Wernig, T. C. Sudhof, Rapid single-step induction of functional neurons from human pluripotent stem cells. *Neuron* **78**, 785–798 (2013).
60. M. Morris, G. M. Knudsen, S. Maeda, J. C. Trinidad, A. Ioanoviciu, A. L. Burlingame, L. Mucke, Tau post-translational modifications in wild-type and human amyloid precursor protein transgenic mice. *Nat. Neurosci.* **18**, 1183–1189 (2015).
61. R. J. Chalkley, P. R. Baker, K. F. Medzihradszky, A. J. Lynn, A. L. Burlingame, In-depth analysis of tandem mass spectrometry data from disparate instrument types. *Mol. Cell. Proteomics* **7**, 2386–2398 (2008).
62. E. Arias, H. Koga, A. Diaz, E. Mocholi, B. Patel, A. M. Cuervo, Lysosomal mTORC2/PHLPP1/Akt regulate chaperone-mediated autophagy. *Mol. Cell* **59**, 270–284 (2015).

Acknowledgments: We gratefully acknowledge all the members of the Kao laboratory for the critical review of the manuscript. In addition, we thank M. Jacobson, D. Agard, D. O. Morgan, and W. Seeley for thoughtful advice. **Funding:** This work was supported by the Rainwater Tau Consortium (A.W.K., T.M., A.M.C., and J.S.Y.), the Paul G. Allen Family Foundation (A.W.K.), the Ramon Areces Foundation (C.A.), the PPG (B.L.M.), and ADRC (A.W.K.). **Author contributions:** C.A. and A.W.K. conceived the project. C.A. performed the molecular biology experiments in cellular models. K.M.S. and T.M.M. designed and performed the experiments in mouse models. A.R.A. generated and banked the patient's fibroblast lines. E.G.G., J.S.Y., E.E.M., B.D., G.D.S., and E.M.R. performed genetic analysis. A.S. and A.M.C. measured autophagy in fibroblasts. K.H.L. and A.L.B. performed the mass spectrometry experiments and analysis. C.A. and A.W.K. wrote the paper with input from many authors. M.D. and D.W.D. provided the human brain tissue samples. B.L.M. recruited the individuals carrying the TSC1 LOF mutation. **Competing interests:** A.M.C. is a cofounder of Selphagy, a program now under Life Biosciences LLC (MA), and consults for Generian Pharmaceuticals Inc. and Cognition Therapeutics Inc. T.M.M. is a consultant for Ionis, Cytokinetics, and Disarm Therapeutics; is a medical advisory board member for Biogen and UCB Pharma; and has licensing agreements with Ionis and C2N. All other authors declare that they have no competing interests. **Data and materials availability:** All data needed to evaluate the conclusions in the paper are present in the paper and/or the Supplementary Materials.

Submitted 2 January 2021
Accepted 17 September 2021
Published 5 November 2021
10.1126/sciadv.abg3897